
Masters Theses

Student Theses and Dissertations

Spring 2016

Particle mediated enhanced mass transfer of diethylhexyl phthalate: A pilot scale system design

Melissa Buechlein

Follow this and additional works at: https://scholarsmine.mst.edu/masters_theses

 Part of the [Environmental Engineering Commons](#)

Department:

Recommended Citation

Buechlein, Melissa, "Particle mediated enhanced mass transfer of diethylhexyl phthalate: A pilot scale system design" (2016). *Masters Theses*. 7498.

https://scholarsmine.mst.edu/masters_theses/7498

This thesis is brought to you by Scholars' Mine, a service of the Missouri S&T Library and Learning Resources. This work is protected by U. S. Copyright Law. Unauthorized use including reproduction for redistribution requires the permission of the copyright holder. For more information, please contact scholarsmine@mst.edu.

PARTICLE MEDIATED ENHANCED MASS TRANSFER OF DIETHYLHEXYL
PHTHALATE: A PILOT SCALE SYSTEM DESIGN

By

MELISSA BUECHLEIN

A THESIS

Presented to the Faculty of the Graduate School of the
MISSOURI UNIVERSITY OF SCIENCE AND TECHNOLOGY

In Partial Fulfillment of the Requirements for the Degree
MASTER OF SCIENCE IN ENVIRONMENTAL ENGINEERING

2016

Approved by

Glenn Morrison, Advisor

Mark Fitch

Fateme Rezaei

© 2016

Melissa Buechlein

All Rights Reserved

ABSTRACT

Phthalates are a class of SVOCs that are widely used as plasticizers and recently epidemiological and toxicological research has found a link between phthalate exposure and increased occurrences of adverse health effects. SVOCs can potentially partition into household dust and airborne particles. Models and micro chamber studies have identified that airborne particles effectively increase SVOC deposition to or emissions from surfaces; SVOCs partition to aerosols in the bulk air, the aerosols then migrate to the surfaces due to eddy and Brownian motion, and then the SVOCs is released inside the SVOC concentration boundary layer adjacent to the surface. Concentration boundary layers limit mass transfer to and from surfaces, but particle mediation of SVOCs effectively decreases this layer thickness, resulting in an increase of the effective mass transfer coefficient. This project focuses on the design and validation of a pilot scale system that will ultimately be used to test model predictions describing this phenomenon. To meet the requirements of the model, there are several requirements: (1) successful generation and characterization of polydisperse particles with an aerodynamic diameter of 10-500 nm at concentrations of 50-100 $\mu\text{g}/\text{m}^3$, (2) quantify the deposition flux of aerosol particles to ensure the particle bound fraction of DEHP will contribute to less than 10% of DEHP flux relative to that due to gas-phase deposition, and (3) quantify the deposition flux of DEHP with a 95% confidence interval less than 30% of magnitude of the flux. The designed system does not meet requirement (2), but does meet requirements (1) and (3). Further work to reduce the particle deposition will need to be done before the system is ready to examine the hypothesis of particle mediation.

ACNOWLEDGEMENTS

First, I would like to thank Dr. Glenn Morrison so much for his invaluable mentorship, expertise, and encouragement throughout my academic career. As a curious student, he was a well-liked professor and has grown to be one of the most influential role models in my life. Without his inspiration and guidance, I would have never even dreamed of accomplishing as much as I have during these years.

Gary and his team were tremendous help in resolving hiccups with the analytical instruments and rectifying plumbing issues that extended outside of my expertise. A great deal of thanks must go out to Max Trueblood for his assistance with the zDMA, CPC, and particle distribution excel sheet. I appreciate Dr. Mark Fitch and Dr. Fateme Rezaei for squeezing me into their hectic schedules to be a part of my committee.

Additionally, I would also like to thank Krista Parker for training me on the majority of the laboratory equipment and best practice methods. The knowledge she has imparted on me is irreplaceable. Hongwan Li, Rebecca Johnson, and Azin Eftekhari have also been a great support whenever I needed them.

Last, but not least, I would like to thank Alex Korff for his continued support and assistance at any given time. He was my cornerstone and helped me push through challenges that arose. Of course, much appreciation goes out to my family for their patience and unconditional love throughout. Without my support of the vast network of friends and family, I could not have accomplished this project. Thank you.

TABLE OF CONTENTS

	Page
ABSTRACT	iii
ACNOWLEDGEMENTS	iv
LIST OF FIGURES	ix
LIST OF TABLES	x
 SECTION	
1. INTRODUCTION	1
1.1. PROPERTIES OF DIETHYLHEXYL PHTHALATE	2
1.2. SVOC EXPOSURE ROUTES	4
1.2.1. Particle Enhanced Exposure Pathways.	5
1.2.2. Phthalate Exposure.....	5
1.2.3. Toxicological Mechanisms in the Body for DEHP Exposure.	7
1.3. AEROSOL PARTICLES	9
1.4. PARTICLE-BOUND SVOC DEPOSITION	12
1.5. GAS-PARTICLE PARTITION COEFFICIENT (K_p).....	13
1.5.1. Partition Coefficient of DEHP.....	14
1.5.2. Equilibrium Time Span for DEHP.....	15
1.6. GAS AND PARTICLE TRANSPORT TO INDOOR SURFACES.....	15
1.7. PARTICLE MEDIATED MASS TRANSPORT	17
1.8. MASS BALANCE ON A THIN VERTICAL SLICE PERPENDICULAR TO FLOW	18
1.9. DESIGN REQUIREMENTS TO TEST THE LIU ET AL. MODEL.....	19
2. GOALS AND OBJECTIVES	21
2.1. OBJECTIVE 1.....	21

2.2. OBJECTIVE 2.....	21
2.3. OBJECTIVE 3.....	21
2.4. OBJECTIVE 4.....	22
3. MATERIALS AND METHODS.....	23
3.1. MATERIALS	23
3.1.1. DEHP.	23
3.1.2. Ammonium Sulfate.....	23
3.1.3. Thermal Desorption Tubes.	23
3.1.4. Metal Coupon.....	23
3.2. EXPERIMENTAL SYSTEM COMPONENTS	24
3.2.1. Experimental Chamber (Box).....	24
3.2.2. DEHP Box Coating.....	25
3.2.3. Particle Generation.....	26
3.2.3.1 Nebulizer.	26
3.2.3.2 Dryer.....	27
3.2.3.3 Bipolar charger.	27
3.2.3.4 Flow control.	27
3.2.3.5 Magnehelic differential pressure gage.	28
3.3. INSTRUMENTATION.....	28
3.3.1. Zimmerman Differential Mobility Analyzer (zDMA) and Condensation Particle Counter (CPC).....	28
3.3.1.1 Zimmerman Differential Mobility Analyzer (zDMA).	28
3.3.1.1.1 Critical particle mobility (Z_p).....	30
3.3.1.1.2 Critical particle diameter (D_p).....	30
3.3.1.1.3 Bin size calculation.	30
3.3.1.1.4 Particle distribution.....	31

3.3.1.2 Condensation Particle Counter (CPC).....	31
3.3.1.3 Particle concentration based on zDMA/CPC.	31
3.3.2. Mass Concentration Based on Filter.	31
3.3.3. Conductivity Probe.	32
3.3.4. Bubble Flow Meter.	32
3.3.5. Relative Humidity Meter.	32
3.3.6. FID-GC/TD.....	33
3.3.6.1 Unity method.	33
3.3.6.2 FID-GC method.....	33
3.3.6.3 Calibration of DEHP using FID-GC/TD.....	33
3.4. ANALYTICAL METHODS	33
3.4.1. DEHP Total Gas Phase Concentration.	35
3.4.2. Calculation of Mass Flux.	35
3.4.3. Calculation of DEHP Mass Flux.....	37
4. RESULTS AND DISCUSSION	38
4.1. TOTAL PARTICLE CONCENTRATION.....	38
4.1.1. Particle Number Concentration.....	38
4.1.2. Differences in Inlet and Outlet Measurement.....	40
4.1.3. Particle Mass Concentration Calculated from Number Concentration.....	41
4.1.4. Mass Concentration Collected on Filter.	44
4.2. PARTICLE DEPOSITION FLUX.....	46
4.3. ESTIMATING DEHP DEPOSITION DUE TO PARTICLE DEPOSITION	50
4.4. DEHP DEPOSITION VELOCITY	51
5. CONCLUSIONS.....	54
5.1. OBJECTIVE 1.....	54

5.1.1. Objective 1 Conclusions.	54
5.1.2. Objective 1 Suggestions for the Future.....	54
5.2. OBJECTIVE 2.....	55
5.2.1. Objective 2 Conclusions.	55
5.2.2. Objective 2 Suggestions for the Future.....	56
5.3. OBJECTIVE 3.....	56
5.3.1. Objective 3 Conclusions.	56
5.3.2. Objective 3 Suggestions for the Future.....	57
5.4. OBJECTIVE 4.....	58
5.4.1. Objective 4 Conclusions.	58
5.4.2. Objective 4 Suggestions for the Future.....	58
REFERENCES	59
VITA	67

LIST OF FIGURES

	Page
Figure 1.1: Particle mediated gas-surface sorption process [34].	18
Figure 3.1: System overview, where DMA is the differential mobility analyzer, CPC is the Condensation Particle Counter, and A.C. is activated carbon.	25
Figure 3.2: Box section view with edge-on view of blade.	26
Figure 3.3: Particle generator and siphon system.	27
Figure 3.4: zDMA flow pattern.	29
Figure 3.5: Blade with attached coupons on aluminum foil covered magnet. The blade has dimensions of 10 inches by 20 inches by 0.25 inches thick.	36
Figure 4.1: Particle Number Concentration for Inlet (a) and Outlet (b) over several different days.	40
Figure 4.2: Particle Outlet Distribution from November 23, 2015.	41
Figure 4.3: Particle Mass Concentration for Inlet (a) and Outlet (b) of Box.	43
Figure 4.4: Particle number concentration data from November 23, 2015. Representing the range of particles captured in a given size bin.	44
Figure 4.5: Mass accumulation of $(\text{NH}_4)_2\text{SO}_4$ per surface area over time.	47
Figure 4.6: $(\text{NH}_4)_2\text{SO}_4$ deposition velocity.	48
Figure 4.7: Particle deposition velocity for experiments with a duration between 70 and 170 hours.	49
Figure 4.8: Mass of DEHP accumulated on metal coupon over time.	52

LIST OF TABLES

	Page
Table 1.1: Structure and Properties of Diethylhexyl phthalate	3
Table 3.1: Unity Thermal Desorber Method.....	34
Table 3.2: FID-GC Method.....	34
Table 4.1: Mass concentration from six different sampling days with the standard deviation of the concentration measurement.....	39
Table 4.2: The size distribution and concentration for typical indoor environments (T), cooking (C), and smoking (S). Mass concentration reported for room except where noted by *. Adapted from [34].	45

1. INTRODUCTION

Building materials, indoor products, and personal care products (PCPs) are widely used in the indoor environment and many of these products contain semi-volatile organic compounds (SVOCs) that are harmful to humans and environmental health. One SVOC, Diethylhexyl phthalate (DEHP), is typically found in polyvinyl chloride (PVC) due to its plasticizing properties [1-13]. DEHP is responsible for a substantial number of health effects due to its toxic effects that include: decreased sperm count, increased incident of allergy and asthma, and increased occurrence of female miscarriages [14-17]. DEHP is non-covalently bonded to the plastic matrix that allows a thin film to develop on top of the material, which acts as a constant emission source for decades [2, 5, 10-12, 18-21].

Aerosol particles are also ubiquitous in the indoor environment from a variety of sources including: cooking, burning candles/incense, or tobacco smoking [13, 22-25]. Particles can penetrate indoors environments due to the variety of outdoor sources, such as: burning of fossil fuels, wildfires, or volcanic activity [23, 24, 26-28]. Once inside, particles can deposit on all interior surfaces and become re-suspended due to human activity [28-30]. The time of year, time of day, building materials, relative humidity, and age of building can dramatically change the profile of aerosol particles throughout the indoor space [18, 23, 24, 28, 29] .

SVOCs can partition to aerosol particles in air or on surfaces that effectively increase the bulk air concentration of SVOCs [1-3, 5, 8, 9, 11, 31, 32]. Higher bulk air SVOC concentrations leads to increased exposure through inhalation and dermal uptake of the particle bound phase. Particle-bound SVOCs can penetrate deeper into human lungs, increasing the effective human exposure risk [4, 7, 9, 33].

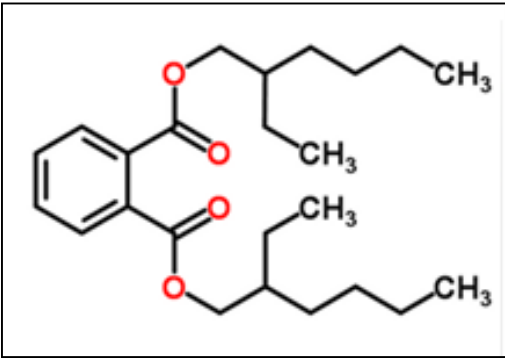
Partitioning of SVOCs to aerosol particles has some effect on the overall enhancement of emission of SVOCs from the surface. Two similar schools of thought exist to explain this phenomenon. One theory is often referred to as shuttling, which predicts that particles become saturated with SVOC in bulk air, then move toward surfaces due to eddy and Brownian motion, and finally release the SVOC inside the SVOC concentration boundary layer. In this instance, particles are not depositing on the surface, but stay suspended in the air phase. The second theory accredits a decrease in boundary layer thickness to the increase of turbulence at the boundary layer, thus resulting in a higher mass transfer coefficient. Increased mass-transfer has been observed in micro-chambers or bench scale processes and modelled for SVOCs [18, 34-37]. However, the mechanisms for the phenomena have not yet been tested at bench or pilot scale. The goal of this research will be to develop a pilot scale (near-full size) system for quantifying the increase in gas-phase mass transfer rates due to the presence of particles. This system would then be used to study mechanisms modelled by Liu et al. [20] or others.

1.1. PROPERTIES OF DIETHYLHEXYL PHTHALATE

The molecular formula of DEHP is $C_{24}H_{38}O_4$ and Table 1.1 identifies its structure and key properties [38, 39]. DEHP is classified as a SVOC based on the vapor pressure at room temperature [3, 7]. Phthalates tend to be hydrophobic and migrate into lipophilic fluids or solids [3]. Characteristics such as the octanol-air partition coefficient (K_{ow}) and the Henry's Law Constant affect whether the compound will partition into liquids or volatilize into air, giving an estimate of potential exposure pathways. As the molecular weight and the length of the alkyl chain increase, the lower the volatility and

water solubility of the phthalate; thereby decreasing the risk of inhalation and increasing the risk for dermal uptake and ingestion [7, 40-44]. These physiochemical properties affect the fate and transport of DEHP in the environment.

Table 1.1. Structure and Properties of Diethylhexyl phthalate

Structure	Properties	
	MW (g/mol)	390.556
	ρ (g/cm ³) at 20°C	0.985
	Log K _{ow}	
	(Log octanol-water partition coefficient at 25°C)	7.6
	Log K _{oa}	
	(Log octanol-air partition coefficient at 25°C)	6.08

After World War II, phthalates were used in the production of PVC as a plasticizer. In particular, DEHP can be incorporated at 20-50% by weight into PVC [3, 45, 46]. Phthalates have been measured in numerous indoor surveys since the 1980s [3]. In 2005, an estimated 5.2 million tons of phthalates were produced [47]. In the early 2000s, phthalates were identified as suspected carcinogens and endocrine disruptors,

affecting reproduction capabilities in males and females, which led to bans on DEHP in Europe and the United States [3, 44, 46].

Phthalates are non-covalently incorporated into the matrix of flexible plastics. The weak Van Der Waals forces break-down over time, allowing the phthalates to leach into foods, soils, and other ecosystem spheres over time. It has been theorized that DEHP forms as a thin film on plastic surfaces that volatilizes at a steady, low rate for many years after installation in the building [2, 5, 10-12, 18-21].

1.2. SVOC EXPOSURE ROUTES

The major exposure pathways for SVOCs include: ingestion, dermal transfer, dermal uptake, and inhalation. Dermal transfer involves skin contact with surfaces contaminated with SVOCs, as a direct uptake pathway. Dermal uptake is of higher concern for SVOCs than VOCs, particularly for compounds that can easily permeate through the skin [6, 7]. Gas phase SVOC concentration affects dermal uptake more than dermal transfer [12, 32]. Ingestion is also of great concern, especially for children, who have a higher tendency to put household items in their mouths. Household dust and indoor surfaces tend to accumulate SVOCs [1, 6, 7, 18]. SVOCs can also migrate into food sources, leading to an increase in ingestion [48].

Clothing, bedding, and hair follicles can sorb SVOCs before settling onto surfaces, collecting as dust. These routes can be ingested, or if loading is high enough, sorbed through the skin [1, 3, 7]. Morrison et al. [49] performed experiments that investigated the effect of clothing on dermal uptake and observed a 2 to 6 fold increase in exposure due to dermal uptake [6].

Exposure to indoor contaminants is related to a wide variety of properties. Source emission properties like initial concentration, partition coefficient, and surface area significantly affect the potential exposure. Increasing the indoor ventilation rate can reduce bulk air concentrations of compounds [10]. Bulk air particle concentrations can affect the dominant exposure pathway and increase the transfer of SVOCs between rooms [10, 32].

1.2.1. Particle Enhanced Exposure Pathways. Due to low volatility of SVOCs, inhalation exposure is often dominated by the particle-bound SVOC [7, 12, 18]. It is speculated that inhalation from this route may account for up to 80% of the total inhaled SVOC and potentially deposit the compounds deeper into the lungs [10, 35]. In addition to increasing inhalation exposure, particles can enhance dermal uptake by allowing the particles which are sorbed with the compounds to deposit onto the surface of the skin, increasing the rate of mass transfer from the air to the skin. Although this phenomenon is not well understood yet, it may play an important role in increasing exposure for SVOCs [7-9, 18].

1.2.2. Phthalate Exposure. Many consumer products contain SVOCs and are brought into the indoor environment. Phthalates are just one of the many SVOCs brought indoors. Phthalates can be detected in food substances, fertilizers, consumer products, indoor and personal air, indoor dust, the environment, and air inside vehicles [42-44, 46, 50, 51].

Higher weight phthalates, like DEHP, tend to be included as additives and plasticizers, while the lower weight species tend to be used as solvents, adhesive wax, ink, pharmaceutical, cosmetic and insecticide productions [3, 43, 44, 50, 52]. In food,

DEHP has been detected at levels as high as 158 mg/kg in oily food jars. Additionally, DEHP was detected in breast milk at 109 ng/L [45]. Due to the incorporation of DEHP in PCPs, women and infants predominantly have a higher exposure to the lower weight phthalates [43, 50]. Patients in the neonatal intensive care units (NICUs) have an estimated 26-fold higher exposure to phthalates compared with an average child due to the multiple medical interventions over time and frequent procedures that employ the use of stored fluids and flexible tubing [44].

The high consumption levels of these compounds have also led to complications in the treatment of waste, detectable levels in surface water and high levels in the soil [42, 46, 47]. The levels in the final sludge from wastewater treatment plants (WWTP) affects the potential for land application as a disposal route [46]. Surface water may have concentrations up to 500 mg/L of total phthalates and phthalic acid esters [53]. This is of concern since DEHP is usually not biodegradable and many plants can uptake these compounds, increasing exposure risk by ingestion when those plants are food sources [42, 47, 53]. Frequently, of the entire phthalate group, DEHP has the highest detection in agricultural soils and vegetables [42, 47]. The average air concentration of DEHP near the German North Sea in 2005 was 0.29 ng/m³ with a particle bound concentration of 1.4 ng/m³ [54]. Many estimates of phthalate human intake have been made; Koch and Calafat [55], reported 0.71-4.6 µg/kg/day of DEHP in German and US populations in 2009 [15].

Langer et al. [3] investigated the dust on non-plastic surfaces in the homes of children and at daycare centers suggesting a positive correlation between the occurrence of allergies and asthma with the fraction of phthalates in the dust. The transdermal route

involves lipophilic compounds diffusing through the epidermis and that directly enter the blood stream to be transported throughout the body without the filtering steps of the intestine or lungs [7]. Skin permeability of phthalates enhances with the increase of alkyl chain length. Since DEHP has lengthy alkyl chains, it has among the highest skin accumulation [43]. DEHP has been observed to accumulate in lipophilic organs, especially or more specifically, in organs with reticuloendothelial functions, such as the liver, spleen, and lungs. [7, 43, 56].

1.2.3. Toxicological Mechanisms in the Body for DEHP Exposure. Since DEHP is lipophilic, toxicity is of higher concern for fatty organs, such as the liver or sex organs. As a result, many studies have investigated the endocrine disrupting abilities (anti-estrogen effects) and carcinogenic processes of phthalate esters, primarily in rodents [14, 57]. The dermal toxicity caused by phthalates is of higher concern due to the high levels of incorporation in PCPs. Pan et al. [43] speculated that phthalates may cause a synergistic, or additive, effect for skin damage based on their evaluation of phthalate dermal toxicity. After the study, Pan et al. [43] determined that DEHP induced cell apoptosis and accumulates in hair follicles. The study also suggested that DEHP causes inflammation of the skin [43]. Ghosh et al. [45] produced a study that identified a route for DEHP to cause hepatotoxicity, toxicity in the liver.

In women, masculinization of the female fetus can be a result if exposed during prenatal development. DEHP and its metabolite, mono-ethyl hexyl phthalate (MEHP), affect the receptor-mediated signaling pathway that produces estradiol in the ovary. This results in an alteration of ovulation times, which may lead to below normal levels of estrogen or potentially polycystic ovaries, which can all lead to decreased female fertility

[14]. Studies have investigated correlations between miscarriages and MEHP levels, human cardiac stress and DEHP exposure, and higher blood pressure during pregnancy and DEHP metabolite excretion, but none of these studies identified any correlations [58, 59]. A study by Ferguson et al. [60] did associate higher DEHP metabolite excretion and preterm birth among US women.

Romani et al. [17] conducted a study to identify a direct negative effect of DEHP on the human reproductive system. This study used human cells to investigate the effect of a number of phthalates on reproductive hormone balance through three different pathways. Their findings suggest DEHP affects female reproduction through a several pathways. DEHP directly inhibits the function of human steroidogenic luteal cells, probably through a receptor-mediated signaling pathway to suppress the production of estradiol. All the studied phthalates influenced the balance of important intraovarian regulators. Interestingly their study suggested that DEHP, itself, could directly affect the inhibition of progesterone (P4), not through the formation of the generally considered more toxic metabolite MEHP. DEHP was determined the greatest reproductive toxicant in this study since it was the only phthalate that exerted a negative influence on the reproduction system via luteolytic $\text{PGF2}\alpha$, which causes premature labor, endometriosis, dysmenorrhea, and other disorders. This was the first study to identify evidence of a direct inhibitory effect of DEHP on mature steroid producing cells [17].

The time of exposure during fetal development can lead to the inhibition of certain hormone signaling transduction, which could result in physical deformity of the testis, as a result of the depressed production of estrogen maintaining hormones. Ultimately, this could reduce sperm count and a decrease in sperm mobility [14, 15].

Due to this potential, many studies have focused on finding an association between earlier pubertal onset, hypospadias, and cryptorchidism, but no associations or only weak associations for humans have been found. The decline in semen quality, referring to count, mobility, or morphology, has been casually associated with phthalate exposure, but clinical relevance has not been determined. Animal studies suggest an association between phthalate exposure and numerous male reproductive deficiencies [15]. In xenografts of rat, mouse, and human testes, multinucleated germ cells were identified, but a decreased production of steroids was only found in rat testes. Human testes seemed resistant, suggesting a different mechanism of action in rats and other mammals [15, 16].

1.3. AEROSOL PARTICLES

Particles are a wide class of indoor components that vary widely in size, composition, and origin. Although particles can transport throughout the indoor environment, there tends to be a higher concentration near the source with a dynamic distribution within a single environment or room [13, 22, 24]. Aerosol particles can also enter commercial buildings via the ventilation ducts and accumulate up to 5 g/m² on surfaces. Older buildings often exceed the local hygiene standards for dust accumulation [29]. Particles with a mean diameter of less than 2.5 µm can be generated indoors from a variety of sources, including: food preparation, generation of heat, pet dander, household electronics, candles, tobacco smoking, humidifiers, and the use of indoor sprays [13, 22-25]. Particles can be re-suspended based on the effect of momentum, turbulent fluctuations, and mechanical dislodgement [28-30].

The specific sources of particles in the indoor environment are highly dependent upon location, building characteristics, the time of year, occupation and activities.

Suburban homes in the UK, near low traffic areas and with no smoking, had an average $PM_{2.5}$ of $6 \mu\text{g}/\text{m}^3$ and an average of PM_1 of $4 \mu\text{g}/\text{m}^3$ during the winter months over a 24 hour collection period. During the summer months, the same homes had an average $PM_{2.5}$ of $15 \mu\text{g}/\text{m}^3$ and an average of PM_1 of $12 \mu\text{g}/\text{m}^3$. As expected, the concentrations varied greatly throughout the day; the highest concentrations occurred when household activities like cleaning, changing clothes, or other types of motion [24]. The windows were open during the summer months, resulting in a significant rise in particulate matter indoors due to the increased penetration factor and enhanced ventilation rate [23, 24].

Relative humidity can affect the size distribution and suspension of particles by affecting the capillary adhesion and electrostatic forces between particles or between particles and surfaces. These forces could increase the deposition of the particles or prevent re-suspension [28]. As a result, homes with a poorly maintained exhaust system in the kitchen could produce particles, especially if there is contact with hot water vapor [61, 62].

Additionally, some gas-phase compounds, like ozone and terpenes, can react to form particles [62]. Some particles originate outdoors as by-products of the burning of fuel sources, vehicle braking, wildfires, volcanic activity, industrial sources and other natural or anthropogenic sources [13, 23, 24, 26-28]. Aerosols can be biological in nature, including infectious agents or bio-allergens [13]. Particles originating outdoors can penetrate the indoors and affect the indoor environment. Over time, the compounds will deposit onto indoor surfaces and walls, but can be re-suspended by indoor activities, such as cleaning, dancing, or walking [13, 22-24, 28, 30, 62-64].

Cooking is one of the most significant sources for indoor aerosols. Cooking can produce particles of concentrations in excess of 2×10^6 #/cm³ near the source. The life-time of an aerosol generated by cooking was found to be 4-6 hours in a study conducted by Hussein et al. [23]. During cooking activities, the living room also had an increase in aerosol concentrations after an initial lag period. Tobacco smoking, another highly significant source for indoor aerosol generation, increased the total particle number concentration 3.6×10^4 #/cm³ over the base-line in the living room of the test house. The result was most significant for particles greater than 30 nm [23]. Smoking can be very dangerous for human health for a number of reasons; the size range of particles emitted can be very particularly hazardous [23, 65].

Through epidemiological studies, relationships have been noted between exposure to particulate and adverse respiratory health, cardiovascular health, asthma, and mortality [23, 66, 67]. Airborne particles smaller than 10 μ m, can be inhaled by humans and deposit at varying depths in the lung. Particles in the size range of 0.05 μ m to 1 μ m deposit in the tracheobronchial region and slightly larger particles, 0.2 μ m to 4 μ m, deposit in the alveolar region of the lungs [33, 65].

Aerosol particles can affect human health on their own, but harmful compounds can sorb to the particles to penetrate deeper in the lungs. For example, one study investigated the re-suspension of polycyclic aromatic hydrocarbons (PAHs) from street dust. The results of this study determined that street dust can be a significant source of PAHs because PAHs bind to the particle fractions [26]. Understanding how SVOCs partition to aerosols will lead to a better understanding of human exposure to these compounds.

1.4. PARTICLE-BOUND SVOC DEPOSITION

Particles can generally be separated into three categories: (1) coarse (aerodynamic diameter greater than 2 μm), (2) fine (aerodynamic diameter between 0.1 and 2 μm), and (3) ultrafine particles (aerodynamic diameter less than 0.1 μm). The three different categories can affect human health and exposure in a variety of ways [7].

The coarse particles settle as dust, which can be re-suspended from floors and other surfaces by human activities. As a result, when SVOCs sorb to these particles, the dust-borne SVOCs redistribute throughout the indoor environment to ultimately settle near people or deposit on people, potentially facilitating a net transport of the dust-borne SVOCs to skin [7]. In New Jersey, average dust settling fluxes were 0.37 $\mu\text{g}/\text{cm}^2/\text{day}$ in the summer and 0.22 $\mu\text{g}/\text{cm}^2/\text{day}$ in the winter [7, 68]. DEHP dust-borne abundances for households in Germany, Japan, and northeast United States approximately range from 1-2 mg/g. The resulting increased exposure could be quite significant [7].

Fine particles typically settle at a much slower rate compared to coarse particles, gaseous species, or ultrafine particles. As a result, fine particles are not as crucial of a factor for influencing dermal exposure and are more likely to increase inhalation exposure. Particles with an aerodynamic diameter between 0.1 μm and 0.5 μm have an average deposition velocity of 0.03 m/hr, approximately two orders of magnitude less than strongly sorbing gaseous species. Assuming an average particle-bound concentration of 100 ng DEHP/ m^3 , the resulting depositional flux to the surface is 72 ng/ m^2/day . Fine particles have a lower depositional flux, of at least an order of magnitude, compared to coarse particles.

Limited knowledge exists about ultrafine particles. Generally, ultrafine particles deposit much more readily to indoor surfaces than fine particles due to their higher

diffusivities and electrostatic attractions. Additionally, these ultrafine particles are generated from localized sources, such as heated surfaces, combustion activities, and gas cooking. These sources are very near to the building occupants, which increases the risk for both dermal and inhalation exposure. In a typical building, with ultrafine particle generating events average 3×10^{13} particles per event, the ultrafine particle deposition to indoor surfaces flux is $0.02 \mu\text{g}/\text{m}^2/\text{day}$. This value is for total ultrafine particles and the actual DEHP deposition would be much less [7].

Chen and Hu [36] modelled the experimental results found by Benning et al. [18] finding that the smaller particles lead to a higher concentration of particle-bound DEHP, resulting in a more serious harm to human health. Chen and Hu [36] also concluded that a larger chamber would result in a higher steady-state concentration of DEHP.

1.5. GAS-PARTICLE PARTITION COEFFICIENT (K_p)

Research has extensively shown that SVOCs, like phthalates, can partition into dust and airborne particles [1-4, 7, 9, 19, 26, 31, 69]. The distribution of a SVOC between the gas-phase and the particle-bound phase is correlated with the vapor pressure of the species and the partitioning coefficient. Typically, species with a vapor pressure greater than 10^{-2} Pa are chiefly in the vapor phase, while species with a vapor pressure less than 10^{-6} Pa exist more commonly in the particle-bound phase. However, SVOCs exist in both phases at varying concentrations [31].

Junge [70] first quantitatively described the partition coefficient (K_p) of SVOCs using gas-solid linear Langmuir isotherm theory. This theory states that the rate of adsorption of a compound to a surface is proportional to the vapor pressure and the available surface area of the particle [31, 69-72]. However, the surface area of a particle

is difficult to determine, which led Yamasaki et al. [73] to assume the surface area is linearly related to total suspended particulate in the atmosphere[31]. Other approaches have looked into the octanol-air partition coefficient (K_{oa}) to parameterize its airborne distribution between the gas and particle phase [9, 31, 69]. Absorption of SVOCs into particles is very dependent on the characteristics of the aerosol, humidity, temperature, and specific chemical properties [69].

It remains unclear which sorption process dominates -absorption or adsorption. Understanding which the foremost process is is essential to characterize the parameters. In the process of absorption, the capacity of the sorbent to partition SVOCs is dependent on the mass or volume of the sorbent. However, in the case of adsorption, the surface area and sorbent-surface interactions are important parameters since the SVOCs partition to the surface of the particle [71].

1.5.1. Partition Coefficient of DEHP. Benning et al. [18] characterized the partition coefficient of DEHP with ammonium sulfate particles in a small emission chamber using vinyl flooring. The K_p was defined as shown in equation (1).

$$\frac{q_{part}}{y \cdot TSP} = K_p \quad (1)$$

Where,

q_{part} -particle-phase DEHP concentration

y -gas-phase DEHP concentration

TSP -total suspended (airborne) particulate mass concentration

They reported a partition coefficient of $0.032 \text{ m}^3/\mu\text{g}$ at 22°C [18]. The partition coefficient reported by Benning et al. [18] can be transformed into a dimensionless

partition coefficient (K_{part}), as reported in Liu et al. [34], by multiplying the K_p by the particle density. This reveals a log K_{part} of 10.7. Weschler et al. [9] summarized the partition coefficients of DEHP to particles based on either the vapor pressure or the K_{OA} 0.25 m³/μg and 0.064 m³/μg, respectively for six phthalate esters, at 25°C.

1.5.2. Equilibrium Time Span for DEHP. Equilibrium of the 45 nm particles with the DEHP is expected to be reached rather quickly, 0.11 minute, based on estimates using equation 4.3 from Weschler and Nazaroff [8] and the K_{OA} from Weschler et al. [9, 18] Using Benning et al. [18]’s dimensionless K_p in place of the K_{OA} , the estimated equilibrium time shifts to 0.14 minute. Liu et al. [34] modelled the equilibrium time for a mean particle diameter of 45 nm to be on the order of 0.1 minute, for the flow rates studied in Benning et al. [18]’s experiment. The equilibrium time span is important to understand, as it varies depending on particle size and species volatility. For the more volatile species, instantaneous equilibrium maybe assumed; however, for the lower volatile species, like DEHP, equilibrium is not instantaneous [74].

1.6. GAS AND PARTICLE TRANSPORT TO INDOOR SURFACES

At the interface between a surface and gas, a more stagnant layer develops as a result of a slower velocity at the surface compared to that in the bulk air. This reduces the convective mixing at the surface, which results in the development of a concentration gradient in a quasi-steady-state layer. The quasi-steady-state nature of the boundary layer means that the characteristic time for diffusion to occur is rate-limiting, as typical in laminar flow situations. Diffusion is defined as the spontaneous mixing of small particles or molecules from regions of high concentration to low concentration. The concentration

profile is primarily influenced by the gas and eddy-diffusivity and not an intrinsic property of the compound itself [34, 37, 75].

Diffusion has been studied extensively in the indoor environment as buildings typically have laminar flow conditions, with diffusion as the main driving force for compounds. Deposition of compounds in the indoor environment is described by an all-inclusive deposition velocity that characterizes the overall mass transfer coefficient limited by diffusion, turbulent (eddy) diffusion, and surface uptake for an overall flux [76, 77]. For more volatile species, like ozone, typical mass transfer coefficients in diffusion driven conditions can range from 0.5-2.7 m/h [78, 79]. Xu and Little [80] reported two different mass transfer coefficients for DEHP that are higher, 1.44 m/hr and 5.04 m/hr. These two values were measured through two different campaigns, the CLIMPAQ and FLEC respectively. The two measurements were done in very different chambers; the FLEC was in a stainless steel chamber while the CLIMPAQ was in a mainly glass chamber [80]. The thickness of the concentration boundary layer also influences the diffusive flux to or from the surface.

The boundary layer thickness is dependent on properties of the specific gaseous species. For particles, the concentration boundary layer is much thinner than for gaseous species. This distinction is important to note because particles can penetrate more deeply into the SOVC boundary layer without diffusion as the driving force. Typically this diffusive boundary layer for gaseous species is on the order of 1-10 mm due to molecular diffusivity being much larger than Brownian diffusivity [8, 79].

1.7. PARTICLE MEDIATED MASS TRANSPORT

The effect of particle mediation to enhance mass transport has been studied extensively across many disciplines [11, 18, 34, 37, 81, 82]. Suspended particles are transported throughout the indoor environment primarily due to eddy and Brownian diffusion [13, 34, 83]. As a result, particle shuttling has been described as one theory to explain particle mediated mass transport. This theory describes particles entering the boundary layer through natural mechanisms, absorbing the compound where the concentration of the compound is high, and desorbing the compound outside of the boundary layer where the concentration of the compound is low. Increased emissions could also occur; the concentration gradient would occur in the opposite directions, causing particles to 'shuttle' the SVOC from the surface into the bulk air [11, 37, 84].

Mass transfer coefficients can be used to analyse diffusion for systems with assumed steady concentration gradients. Particles are predicted to decrease mass transfer coefficients or increase the interfacial surface area [37, 84]. Depending on the solids loading, size and surface properties, particles can increase the mass transfer coefficient by enhancing turbulence at the interface. The enhanced turbulence also affects the thickness of the quiescent concentration boundary layer, effectively increasing the mass transport of a compound into the bulk air [11, 12, 18, 34]. The particles of the highest interest to enhance the mass transfer of DEHP have a size bin of less than 200 μm [2]. According to Nazaroff [13], these particles would be classified as ultrafine, typical of gas cooking or tobacco smoke- organic in composition.

1.8. MASS BALANCE ON A THIN VERTICAL SLICE PERPENDICULAR TO FLOW

Liu et al. [34] performed a mass balance on a thin vertical slice perpendicular to the direction of the flow to describe particle mediated mass transfer. Figure 1.1 is an illustration from Liu et al. [34] that visually represents the concentration gradient of DEHP at the surface to the surface. This concentration gradient is the driving force within the model, assuming deposition is occurring [34].

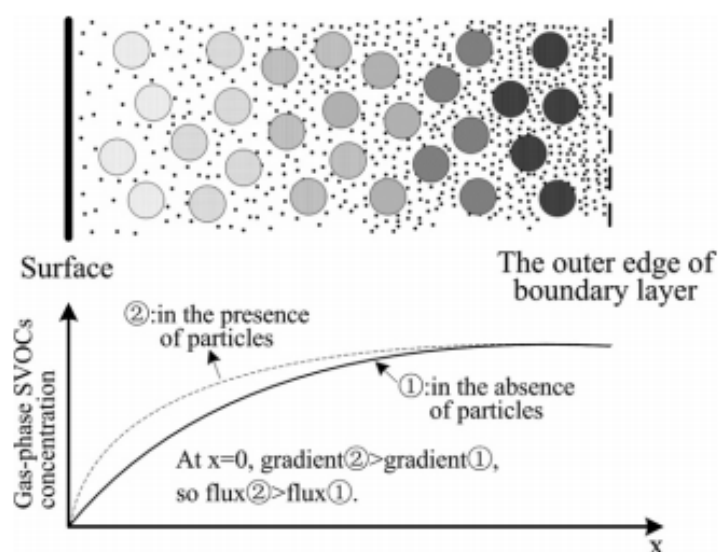


Figure 1.1: Particle mediated gas-surface sorption process [34].

They assumed instantaneous equilibrium between the particle and DEHP gas concentrations, treating the particle as a well-mixed compartment. Within the slice, the partition coefficient (K_{part}) governs the transfer of SVOCs between the gas-phase and particle-bound phase. This model supports the idea of particle mediated mass transfer for both mono-disperse and poly-disperse particles, with the largest effect seen for particles

in the 10-500 nm range. Lower volatility compounds will be most affected by the particle mediation, especially when the air concentration of particles is highest. They predicted that during realistic indoor conditions, SVOC inhalation dose could be increased by a factor of 4-10 [34].

1.9. DESIGN REQUIREMENTS TO TEST THE LIU ET AL. MODEL

The design of a pilot scale system to examine the Liu et al. [34] mass balance model would need to meet several requirements.

- To test the Liu et al. [34] model, it is important to observe DEHP flux to surfaces in a system that is similar in scale to a room, but practical for laboratory studies. The residence time should be sufficiently long for particles to equilibrate with DEHP present at the inner surfaces of the chamber, but not so long that particle deposition loss to surfaces reduces the concentration of particles below the required level (see next bullet).
- The particle concentration will need to be high enough in the 10-500 nm to test this mechanism. The effect must be significant enough to measure an increased mass of DEHP to the surface after excluding the mass deposited directly by particle deposition. Based on Benning et al. [18], the effective partition coefficient between DEHP and ammonium sulfate aerosols of this size range is $0.032 \text{ m}^3/\mu\text{g}$, or in unitless form used by Liu et al. [34], 5×10^{11} . To be able to observe a 50% increase in flux in the presence of polydisperse particles, Liu et al. [34] predicts that the particle concentration would need to be about $50\text{-}200 \mu\text{g}/\text{m}^3$. Therefore, this is the design goal for particle concentration.

- Particle bound DEHP can contribute to surface uptake when these particles deposit on the surface. This effect should be sufficiently small, less than 10%, to negligibly contribute to overall DEHP deposition.
- To be able to observe a 50% increase in the DEHP deposition rate, the method should be sufficiently sensitive and reproducible to distinguish a 50% increase in mass on surfaces used to make this measurement. Thus the relative standard deviation for repeated measurements should be less than about 25%. This is the design target for the DEHP deposition flux measurement.

2. GOALS AND OBJECTIVES

The results of previous studies indicated that particles can enhance mass transfer of DEHP from the air to surfaces. The goal of this study to develop a system that can be used to quantify the effective mass transfer coefficient of DEHP to the surface of a flat plate in the presence and absence of aerosol particles in a pilot scale study. The system is intended to test the Liu et al. [34] enhanced mass transfer model. To separate out the effect of DEHP accumulation on a surface due to particle deposition, both DEHP and particle mass deposited must be measured. The following objectives were determined to verify that the design of this system will test this hypothesis.

2.1. OBJECTIVE 1

Construct a chamber to test the Liu et al. [34] model.

2.2. OBJECTIVE 2

Construct a particle generator that can deliver a sufficiently high concentration ($50\text{--}100\text{ }\mu\text{g}/\text{m}^3$) of polydisperse particles in the appropriate size range (10-500 nm in aerodynamic diameter) to test the Liu et al. [34] model.

2.3. OBJECTIVE 3

Quantify the deposition flux and deposition velocity of the aerosol particles to metal coupons. Demonstrate that the DEHP deposition associated with particle deposition (particle bound DEHP) contributes to less than 10% of DEHP flux relative to that due to gas-phase deposition.

2.4. OBJECTIVE 4

Quantify the flux and estimate the deposition velocity of DEHP to metal coupons.

Demonstrate that the flux is sufficiently reproducible to test the Liu et al. [34] model, that the 95% confidence interval is less than 30% of magnitude of the flux.

3. MATERIALS AND METHODS

The following methods were used to verify that the system would operate in a way that the hypothesis of aerosol mediated enhanced mass transfer of DEHP to surface could be tested in a pilot scale system and meet the objectives of this project.

3.1. MATERIALS

DEHP, ammonium sulfate, thermal desorption tubes, and metal coupons were used to complete this project.

3.1.1. DEHP. $\geq 99.5\%$ Dioctyl phthalate (DEHP) was purchased through Sigma Aldrich catalog number D201154. The DEHP was applied thinly to all walls directly inside of the stainless steel box to provide a constant emission source throughout the experiment.

3.1.2. Ammonium Sulfate. Ammonium sulfate was purchased through Sigma Aldrich catalog number RES1427A-A7. A 1 gram ammonium sulfate per liter Milli-Q purified water solution was used in the nebulizer to aerosolize the ammonium sulfate particles.

3.1.3. Thermal Desorption Tubes. Thermal desorption tubes filled with 3.13 ± 0.25 cm, or 63.6 ± 6 mg, glass wool and 35 ± 2.6 mg of Tenax TA were used to measure the air concentration of DEHP.

3.1.4. Metal Coupon. Stainless steel coupons were cut in the machine shop of the Structural Engineering Research Laboratory at Missouri University of Science and Technology. The metal coupons are 8 cm by 0.4 cm by 0.1 cm thick resulting in a total exposed surface area of 3.2 cm^2 per coupon.

3.2. EXPERIMENTAL SYSTEM COMPONENTS

The experimental apparatus, as seen in Figure 3.1, was designed to provide a large volume to surface area ratio in order to limit the particle deposition by minimizing wall effects (a large cube). Filtered compressed air controlled by a line regulator at 30 psi was forced into the nebulizer to produce small droplets of ammonium sulfate solution. The particle stream passed through a dryer to remove moisture and form solid ammonium sulfate particles. Then the stream passed through a bipolar charger to achieve a neutral (average) charge on the particles. As the dryer aged, the relative humidity increased which potentially reduced the effectiveness of conversion of droplets to salt particles; therefore it was measured periodically to ensure the air stream was not too wet. Valves were placed before and after the box to allow flow from either the inlet or outlet to measure total suspended particle (TSP). Throughout the experiments, a blade was inserted through the lid with attached coupons to limit disruption to the system during sampling, as seen in Figure 3.2. Flow through the system was controlled by a needle valve attached to the vacuum plumbing; stability of the system flowrate was determined with a magnehelic differential pressure gage.

3.2.1. Experimental Chamber (Box). To meet Objective 1, the main chamber was designed to reduce the surface-area to volume ratio (a cube) to minimize particle deposition. It was the largest cube-shaped box that would fit into the available climate controlled chambers. Based on these considerations, a box measuring 0.86 meters on a side was constructed. The 644 L steel box, shown in Figure 3.2, was welded by the Missouri University of Science and Technology Civil Engineering machine shop. The lid was sealed with a rubber gasket fastened between the lid and box by 72 bolts. The

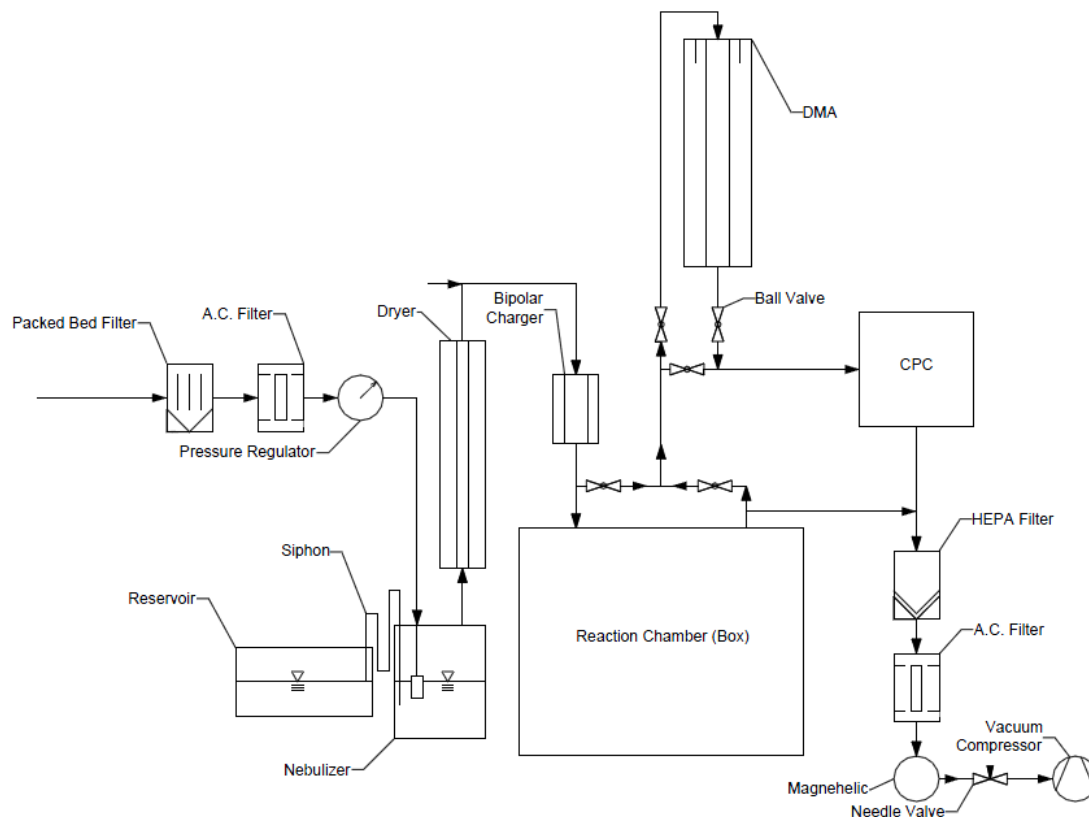


Figure 3.1: System overview, where DMA is the differential mobility analyzer, CPC is the Condensation Particle Counter, and A.C. is activated carbon.

whole lid was not removed throughout the experiment and sampling was conducted through a slot in the lid to reduce disturbance of the chamber air. A blade was inserted into the slot during the experiments, as seen in Figure 3.2. The metal coupons were magnetically held onto the blade by a magnet covered in aluminum foil.

3.2.2. DEHP Box Coating. The $\geq 99.5\%$ DEHP was applied to a Kimwipe attached to the head a Swiffer[®] and thinly spread across all of the walls and bottom of the box.

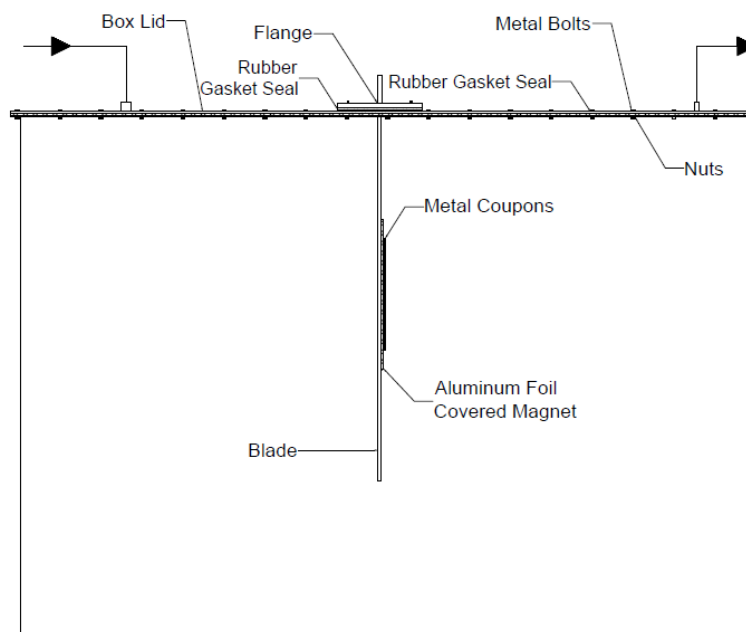


Figure 3.2: Box section view with edge-on view of blade.

3.2.3. Particle Generation. The particles were generated using a nebulizer. To isolate the salt particle, the particle stream passed through the drier. Next, the particles passed through a bipolar charger to obtain an overall neutral particle stream.

3.2.3.1 Nebulizer. A particle generator was constructed using a mason jar that had two holes drilled in the lid, as depicted in Figure 3.3. One hole was 0.5-in in diameter and allowed air to exit the generator. The other hole was 0.25 inches in diameter and allowed the compressed air to enter the generator. The siphon line was feed through the 0.25-in diameter tubing to maintain a constant level of solution. The outlet of the 0.25-in hole had a nebulizer used to aerosolize the 1.00 g/L ammonium sulfate solution.

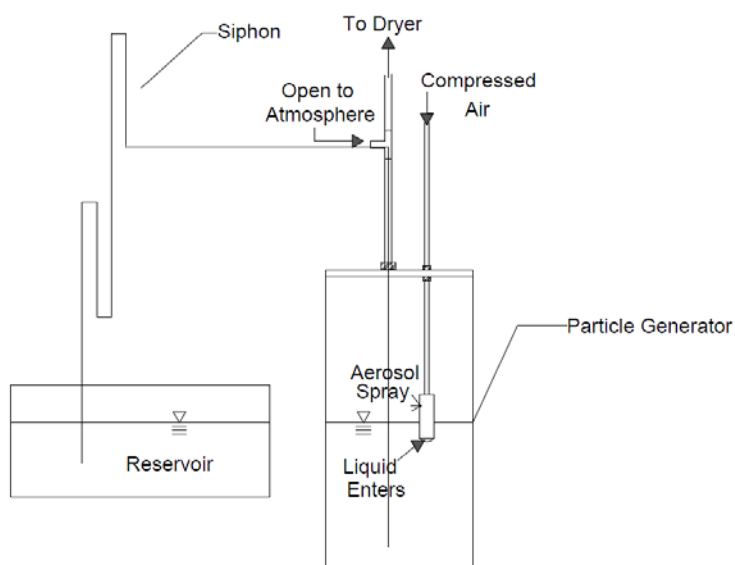


Figure 3.3: Particle generator and siphon system.

3.2.3.2 Dryer. The dryer was constructed using a clear PVC cylinder with a diameter of 9 cm and 70 cm long filled with Drierite (with indicator 10-20 mesh). A 1-in. diameter mesh screen cylinder was placed in the center to allow air and particles to move through.

3.2.3.3 Bipolar charger. A bipolar charger was used to provide an overall neutral charge for the ammonium sulfate particles.

3.2.3.4 Flow control. The flow through the system was maintained with a vacuum pump. The flow was set by a needle valve after a series of filters. A magnehelic differential pressure gage was used to monitor the vacuum flowrate. To meet the requirement of Objective 1, the residence time of the main experimental chamber (box)

was approximately five hours; this was estimated to be sufficiently long to allow particles to achieve ~90% of equilibrium with DEHP that coats the inner wall of the box.

3.2.3.5 Magnehelic differential pressure gage. A simple ¼-in. needle valve was used to control the vacuum draw through the system. To ensure this remained constant, the magnehelic differential pressure gage was connected in line directly before the valve and recorded daily.

3.3. INSTRUMENTATION

The following instrumentation was employed to determine the particle concentration distribution, particle deposition velocity, the system flow rate, relative humidity and DEHP mass. The above listed parameters were important to quantify the mass transfer of DEHP to the surface of the metal coupons due to particle phase deposition versus gas phase concentration.

3.3.1. Zimmerman Differential Mobility Analyzer (zDMA) and Condensation Particle Counter (CPC). Figure 3.4 depicts the flow pattern and voltage across the zDMA. As can be seen in this figure, a sheath flow (Q_{sh}) at 0.3 L/min is drawn through the zDMA and a poly flow (Q_{poly}) at 28.5 L/min is recycled through the zDMA by a pump and mass flow controller. The Q_{sh} contains the particles from the box system. This flow rate is controlled by an oil-free vacuum rotary pump in the CPC. The exhaust of the CPC was connected back to the system line before the HEPA filter as seen in Figure 3.4.

3.3.1.1 Zimmerman Differential Mobility Analyzer (zDMA). A zDMA was borrowed from the Center of Excellence for Aerospace Particulate Emission Reduction Research Laboratory at Missouri University of Science and Technology. The following

subsections describe how to relate the voltage applied to the zDMA to the particle diameter and bin size.

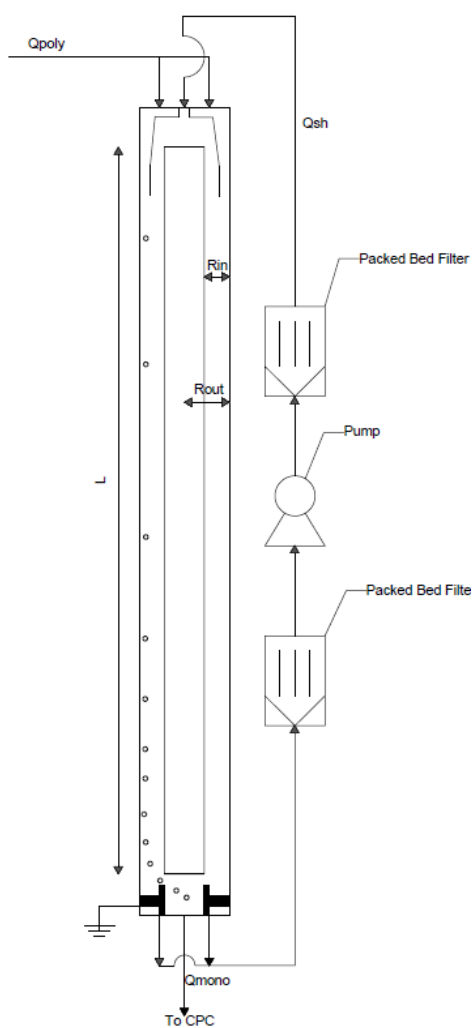


Figure 3.4: zDMA flow pattern.

3.3.1.1.1 Critical particle mobility (Z_p). The voltage applied across the zDMA, combined with the Q_s and zDMA dimensions, determines the critical particle mobility (Z_p). Equation (1) displays the calculation of Z_p [27].

$$\frac{Q_s}{2\pi VL} \ln \frac{r_{out}}{r_{in}} = Z_p \quad (1)$$

Where,

r_{out} - outer diameter of the zDMA (4.4 cm)

r_{in} - inner diameter of the zDMA (2.5 cm)

L - length of the zDMA (72.8 cm)

V - voltage (volts)

3.3.1.1.2 Critical particle diameter (D_p). The critical particle diameter (D_p) is expressed by equation (2).

$$\frac{n * e * C_c}{3 * \pi * \eta * \chi * D_p} = Z_p \quad (2)$$

Where,

η - loss correction coefficient

χ -dynamic shape factor

n -number of elementary charges a particle has

e - elementary charge

C_c -Cunningham Slip Correction factor

3.3.1.1.3 Bin size calculation. The ratio of Q_s/Q_{poly} multiplied by D_p yields the bin size (ζ), as expressed by equation (3).

$$\frac{Q_s}{Q_{poly}} * D_p = \zeta \quad (3)$$

3.3.1.1.4 Particle distribution. The voltage across the zDMA was systematically changed in a randomized order. At each voltage, 20 concentrations were recorded over five minutes. The average of these concentration values was taken as the concentration at that voltage [27].

3.3.1.2 Condensation Particle Counter (CPC). A TSI 3022A CPC was borrowed from the Center of Excellence for Aerospace Particulate Emission Reduction Research Laboratory at Missouri University of Science and Technology.

3.3.1.3 Particle concentration based on zDMA/CPC. The total particle number concentration was determined through the use of the zDMA and CPC. Air was drawn from the inlet or outlet of the box to the zDMA at 0.3 L/min, controlled by the CPC vacuum pump. This system provides a number concentration for particles with diameters between values dependent on the voltage applied to the zDMA. By varying voltage (described in more detail below), the concentration for the entire size distribution (particle diameter distribution) is determined. To verify that the total mass concentration determined by integrating all size “bins” was correct, particles were also collected on a filter.

3.3.2. Mass Concentration Based on Filter. As a check on the estimated concentration based on the zDMA/CPC system, a Fluoropore membrane filter (47mm, PTFE, pore size 0.025 μm) was connected to the inlet of a smaller 5 gallon bucket. The box was already coated at the time this check was employed and the flux of DEHP should be characterized before the introduction of particles into that system.

A vacuum air sample was drawn through the filter long enough to collect ~20 L. The filter and 40 mL of MilleQ water were placed on a shaker tray for 20 minutes. Then,

the conductivity of the solution was measured and used to determine the ammonium sulfate concentration based on prior calibration of the conductivity meter. The mass deposited on the surface of the filter was calculated based on the concentration of the solution. This mass was divided by the volume of the sample to determine the total mass concentration of particles.

3.3.3. Conductivity Probe. The Traceable Digital Conductivity Meter was purchased from Fischer Scientific and used to determine the concentration of liquid extracted particle samples. The range for this meter is $0.1\mu\text{S}/\text{cm}$ to $200\mu\text{S}/\text{cm}$, with an accuracy of $\pm 0.4\%$ full scale.

3.3.4. Bubble Flow Meter. A bubble flow meter was constructed to measure the flowrate through the system. In each column, 500 mL were marked with a line at the upper and lower limit. Soapy water was inserted into the bottom of each column using a squirt bottle. The flow was connected with the vacuum side on the top and the positive flow on the bottom. Once the columns stabilized, the time for one bubble to pass from the bottom line to the top line was measured. The average of four timed bubbles was used to calculate the flowrate for each column individually. The average flowrate for each column was added together to obtain the total flowrate.

3.3.5. Relative Humidity Meter. A Pen-type Digital Thermo-Hygrometer, like the one from rp electronics SKU: 5590, was used to ensure effective operation of the dryer system. It has a humidity range of 2% to 98% with an accuracy of $\pm 5\%$.

3.3.6. FID-GC/TD. Agilent model 6890 Series Gas Chromatograph (GC) with Flame Ionization Detector (FID) equipped with a UNITY Thermal Desorber with Ultra TD auto sampler purchased from Markes International was used to analyze the DEHP on the sorption tubes and deposited on the metal coupons.

3.3.6.1 Unity method. The method for the thermal desorption system is represented in Table 3.1. Each tube underwent three injections. The responses of the first two injections were summed for the total response. The third injection was insurance that the whole sample was collected on the first two desorption.

3.3.6.2 FID-GC method. Table 3.2 is the method for the FID-GC. The sample from the thermal desorber was automatically injected onto the FID-GC, initiating the program to run.

3.3.6.3 Calibration of DEHP using FID-GC/TD. The FID-GC/TD was calibrated by spiking a known mass of DEHP onto the quartz wool sorption tubes. A 100 ng/μl DEHP in 1% ethyl acetate in hexane solution was prepared. A total of five different masses were used to develop the calibration curve: 0 ng, 25 ng, 50 ng, 100 ng, and 200 ng.

3.4. ANALYTICAL METHODS

The following analytical methods were employed to calculate the total DEHP gas phase and unbound DEHP gas phase concentration, mass flux, particle deposition velocity, the DEHP mass accumulation and the DEHP mass accumulation due to particles.

Table 3.1 Unity Thermal Desorber Method

Parameter	value
Thermal desorber	
<i>Primary desorption (sorbent tube)</i>	
Temperature	290 °C
Time	15 min
Gas flow	30 mL/min
Split	Off
Trap	20 °C
<i>Secondary desorption (cold trap)</i>	
Packing material	Unsilanised glass wool
Temperature	300 °C
Time	3 min
Split	10 mL/min
Transfer line	185 °C

Table 3.2: FID-GC Method.

Parameter	Value
GC-FID	
<i>GC Oven</i>	
Temperature	40 °C for 1 min, 40 °C/min to 300 °C, hold 5 min
GC Constant Pressure	6 psi
Column	HP-5 5% Phenyl Methyl Siloxane (0.32 mm x 30 m x 0.25 µm)
Carrier Gas	Nitrogen
<i>FID (detector)</i>	
Temperature	300 °C
Air Flow	450 mL/min
H ₂ Flow	40 mL/min

3.4.1. DEHP Total Gas Phase Concentration. The gas-phase concentration of DEHP in the box was to be determined by drawing 50 mL/min through a sorbent tube from one of the sampling ports on the box. Samples and duplicates were to be taken for approximately 24 hours, for a sample volume of 72 L. The samples were then to be analyzed on the FID-GC/TD. The mass collected on the sorption tube divided by the volume of the sample was determined as the concentration of DEHP inside the box. Unfortunately, the tool for quantifying the DEHP (Thermal Desorber, GCFID) broke down soon after preparing (coating) the box with DEHP. It was not fixed by the time this thesis was completed.

3.4.2. Calculation of Mass Flux. The mass flux of particles to the metal coupons was determined by calculating the mass deposited onto the coupons over a given time span with a known surface area. This flux was used to calculate the particle deposition velocity (v_{d_part}). Coupons were magnetically secured to the blade, as depicted in Figure 3.5. The coupons were allowed to collect particles for a period of time (t). The coupons were carefully handled by forceps and placed into a 40 mL vial. 10 mL (v) of MilleQ water was added to the jar. The vials were put on a shaker tray for 20 minutes to ensure the solutions were well mixed. The conductivity of the solution was measure using the conductivity probe.

The conductivity of the solution was measured and compared against the calibration of known standard solution concentrations. Based on the sample concentration (C) and extraction volume (v), the mass deposited (m_{part}) was determined using equation (9).

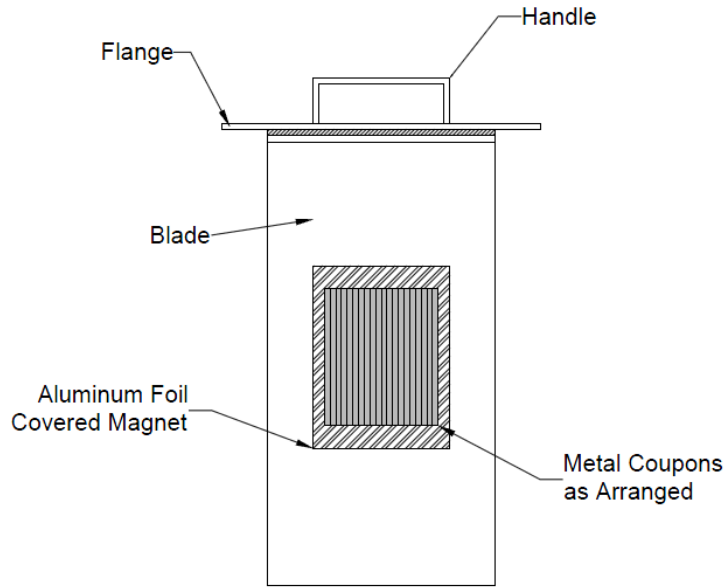


Figure 3.5: Blade with attached coupons on aluminum foil covered magnet. The blade has dimensions of 10 inches by 20 inches by 0.25 inches thick.

The mass flux (J_{part}) was calculated using equation (5).

$$C \cdot v = m_{part} \quad (4)$$

$$J_{part} = \frac{m_{part}}{t \cdot SA} \quad (5)$$

Where,

SA - Surface Area Exposed on Coupon

The m_{part} was then used to determine deposition velocity (v_{dp}) of particles to the coupon surface (6).

$$v_{dp} = \frac{J_{part}}{TSP} \quad (6)$$

3.4.3. Calculation of DEHP Mass Flux. The mass flux of DEHP to the surface was measured in a similar fashion to the measurement of mass flux of particles. The clean coupons were placed in a small 1.4 L chamber for an amount of time (t). Upon removal, the mass of DEHP deposited was determined using the FID-GC/TD. The response was compared with the calibration curve to determine the mass (m_{DEHP}) desorbed from each coupon. The flux was then determined based on equation (8).

$$J_{DEHP} = \frac{m_{DEHP}}{t \cdot SA} \quad (7)$$

Where,

SA - Surface Area Exposed on Coupon

The deposition velocity was then determined using equation (8).

$$v_{dD} = \frac{J_{DEHP}}{C_{DEHP}} \quad (8)$$

Where,

C_{DEHP} is the gas phase air concentration of DEHP ($\mu\text{g}/\text{m}^3$)

Note that due to analytical problems in measuring the gas concentration of DEHP, the gas concentration was estimated to the saturation concentration at the temperature of the experiment.

4. RESULTS AND DISCUSSION

The results from this investigation demonstrate that the system is partially ready for testing the Liu et al. [34] model. This section will detail the results from this study and typical values found throughout the literature.

4.1. TOTAL PARTICLE CONCENTRATION

Prior to each sampling of particle deposition, a particle distribution was measured for the inlet of the box and outlet of the box. The distribution was used to estimate the mass concentration within the box and identify the mean particle diameter. Previous work indicated that the mass transfer for SVOCs would be enhanced in the presence of particles less than 200 nm in aerodynamic diameter [11]. Therefore, it was essential that enough particles in the size range of interest were created, roughly 50-100 $\mu\text{g}/\text{m}^3$ with aerodynamic diameters in the range of 10-500 nm according to the Liu et al. [34] model. The inlet and outlet mass concentrations can be seen in Table 4.1 from six different days. It is expected that the mass concentration at the outlet measured by the zDMA/CPC underestimate the mass concentration based on mass concentrations of the inlet stream measured using the Fluoropore membrane filter. The filter mass concentration based on the filter measurements is $2700 \pm 460 \mu\text{g}/\text{m}^3$, which is higher than the highest inlet mass concentration value based on the particle distribution.

4.1.1. Particle Number Concentration. The results of the inlet particle number concentration and outlet particle number concentration are shown in Figure 4.1, and Table 4.1, from six different sampling dates. Although the specific concentrations vary, the mean particle diameter, based on the diameter with the highest particle number

Table 4.1: Mass concentration from six different sampling days with the standard deviation of the concentration measurement.

	Inlet		Outlet	
Date	Average Concentration (ug/cm ³)	Standard Deviation	Average Concentration (ug/cm ³)	Standard Deviation
150813	828	0.9	41	0.1
150817	555	0.6	52	0.2
150825	395	0.5	78	0.3
151112	516	17	187	16.6
151116	823	1.9	176	0.5
151123	1545	4	265	3.2
Average	777.0	414.2	133.2	89.7

concentration, did not change dramatically. For the inlet, the mean particle diameter was about 85 nm. For the outlet, this size was slightly higher, around ~105 nm. This shift in peak particle diameter was probably due to agglomeration of particles while inside of the box [13].

The number concentrations within the inlet and outlet measurements are highly variable, which is probably due to a natural variation of the system. To emphasize the gaps in the particle size bin, the data from the outlet of the box collected on November 23, 2015 is represented in Figure 4.2. Despite the missing particle sizes, the smooth curvature of the line allowed an estimation of the particle total concentration. In Figure 4.2, the horizontal error bars represent the anticipated bin size and the vertical error bars are the standard deviation of the 20 recorded particle concentrations of that bin.

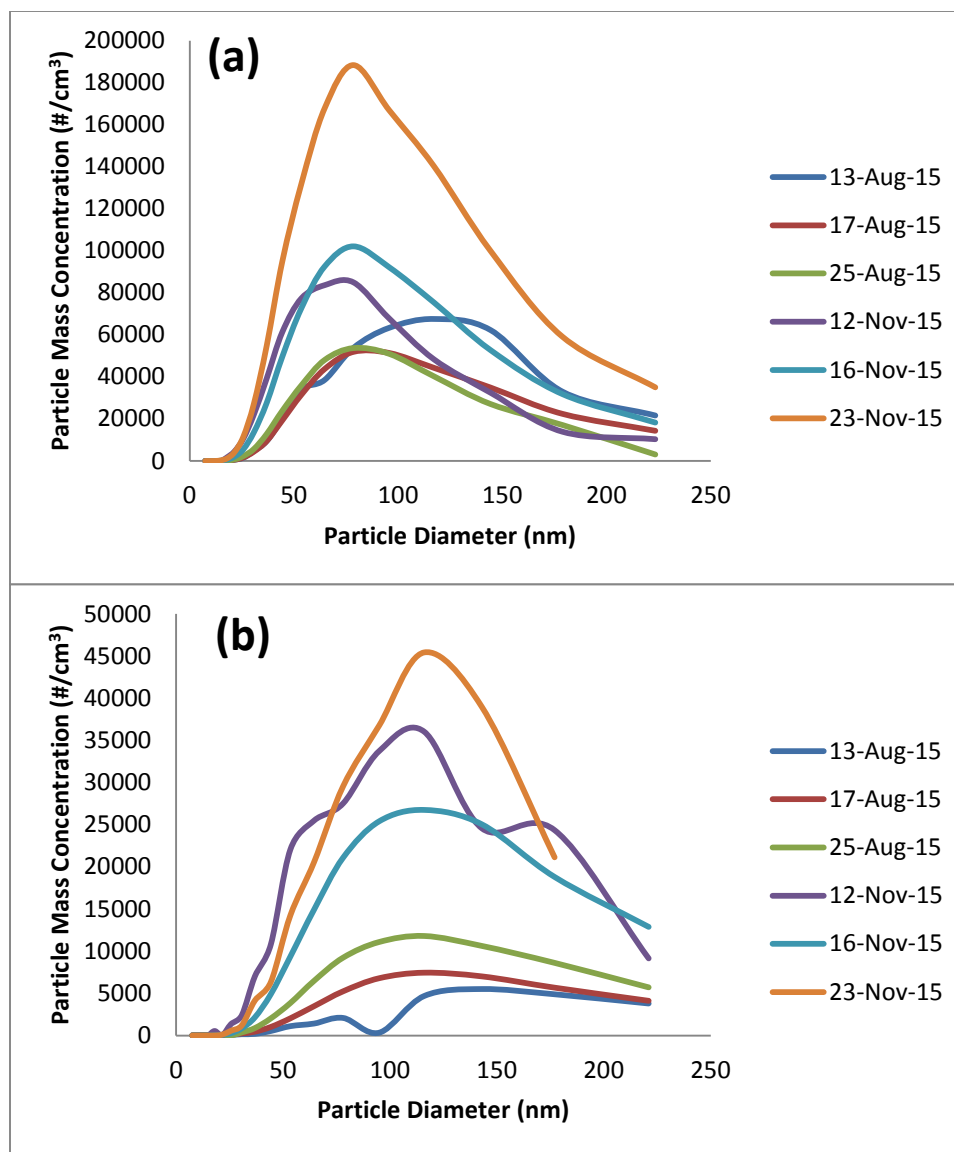


Figure 4.1: Particle Number Concentration for Inlet (a) and Outlet (b) over several different days.

4.1.2. Differences in Inlet and Outlet Measurement. The large difference in the inlet and outlet concentrations was attributed to a variety of losses. Within the box, deposition of the particles to the surfaces represents the largest loss mechanism. Another

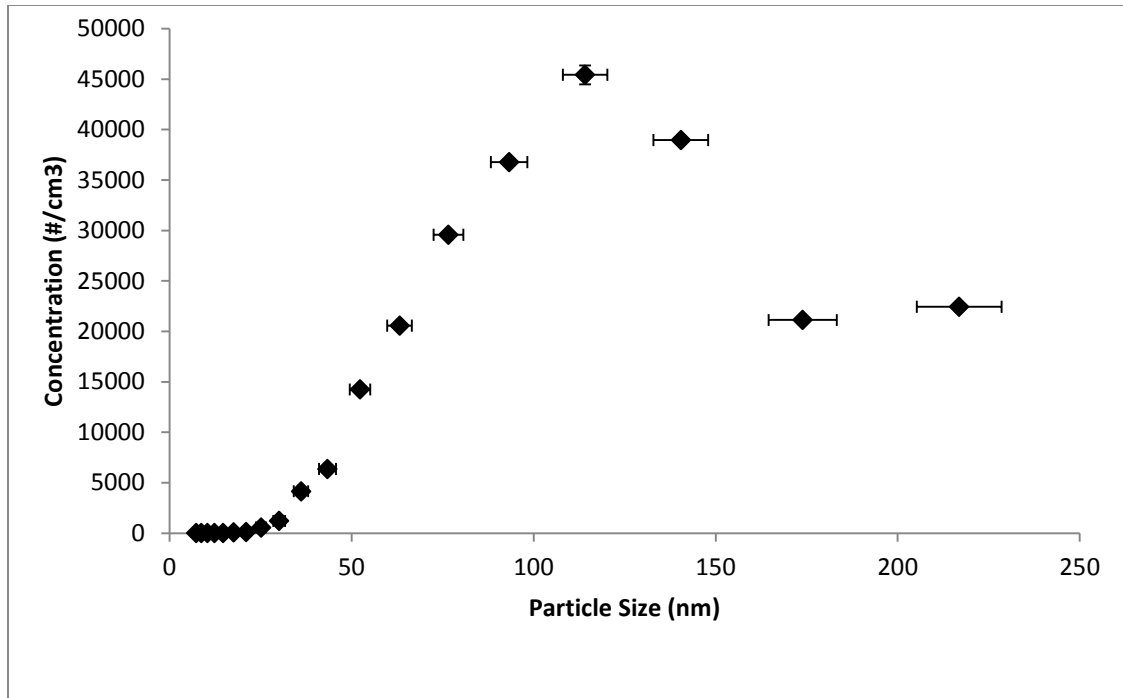


Figure 4.2: Particle Outlet Distribution from November 23, 2015.

reason the outlet concentration was lower than the inlet is due to particle agglomeration within the box. This would shift the particles to larger diameters and some mass is shifted into a bin size that was not detectable using the zDMA, since the highest measurable diameter was ~230 nm.

4.1.3. Particle Mass Concentration Calculated from Number Concentration.

The particle mass concentration was determined for calculations of deposition velocity experiments. Initially, the mass concentration was calculated using equation (9) from the number concentration assuming the median particle diameter is the mean particle diameter and spherical particles, with a constant particle density.

$$\overline{TSP} = \sum_{i=1}^n \rho \cdot \bar{V}_i \cdot \overline{C_{N,i}} \quad (9)$$

Where,

ρ -particle density (g/cm³)

V_i -size bin average particle volume, assuming a sphere (cm³)

C_{Ni} -size bin average particle number concentration (#/cm³)

Figure 4.3 represents the inlet and outlet mass concentration for the six different sampling dates. The variations between the six different sampling dates is further emphasized here and the inlet and outlet concentration differences become more apparent.

To gain a total particle mass concentration, the mass concentration for each bin was summed. Figure 4.4 depicts the data from November 23, 2015 with the column thickness representing the range of particles covered in each of the bin sizes, with a column height of the associated number concentration. Some bins are not represented in this data and considered missing. If the widths of these bin sizes are actually smaller than approximated by equation (3), then the total mass concentration could be much higher. The missing bins were assumed to have a concentration that was the average of the bin size before and after it and the average particle diameter was the median between the bin sizes. Using this approximation, the inlet and outlet number concentrations were converted into mass concentrations, as shown in Table 4.1. Benning et al. [18]

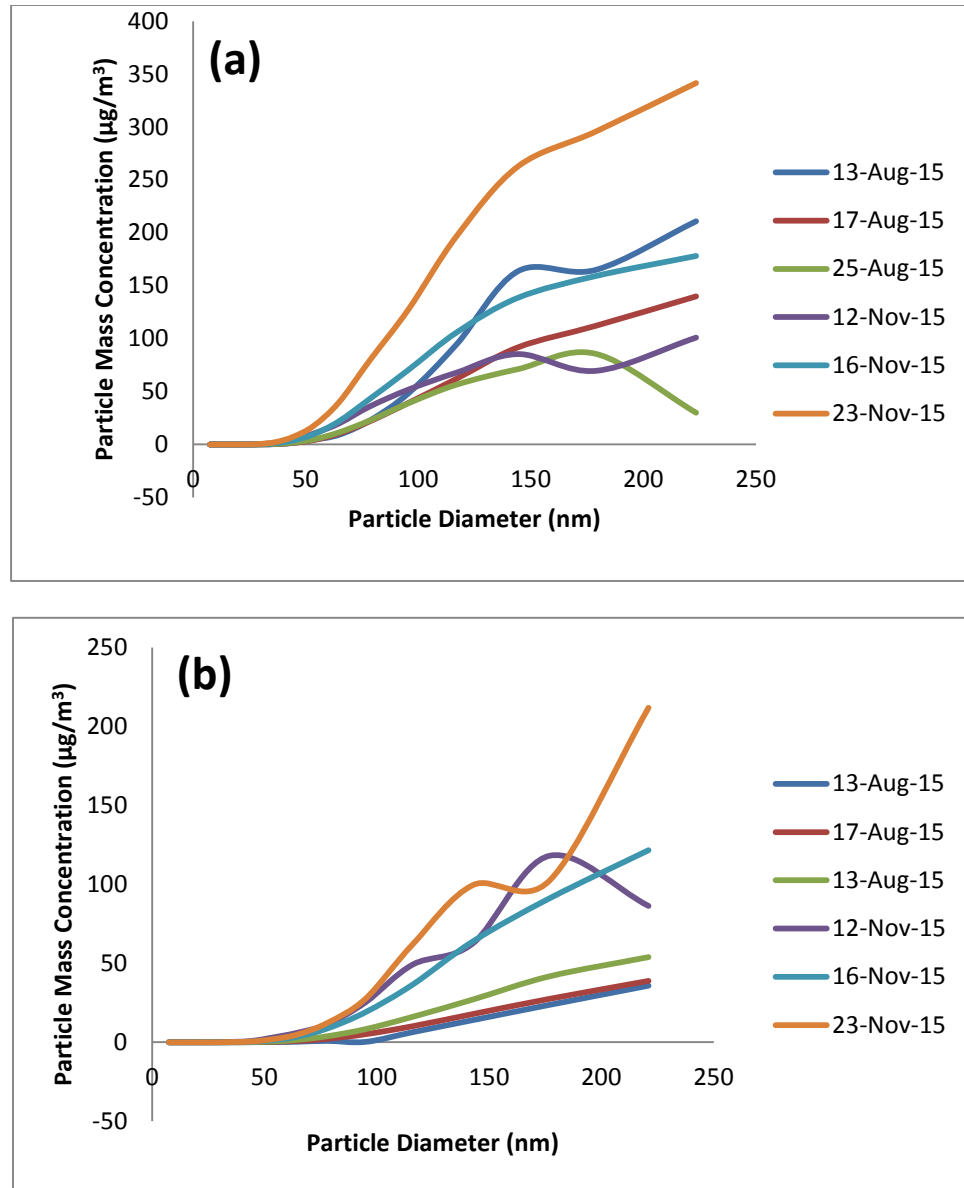


Figure 4.3: Particle Mass Concentration for Inlet (a) and Outlet (b) of Box.

effectively conducted a small scale similar experiment with an inlet air concentration between 395 and 1545 $\mu\text{g}/\text{m}^3$; however, Liu et al. [34] modeled the phenomena with an air concentration on the order produced in this experiment, as determined by this method of measurement [11, 18].

Table 4.2 represents typical indoor concentrations from various sources. Liu et al. [34] used both directly measured values from Nazaroff [13], See and Balasubramanian

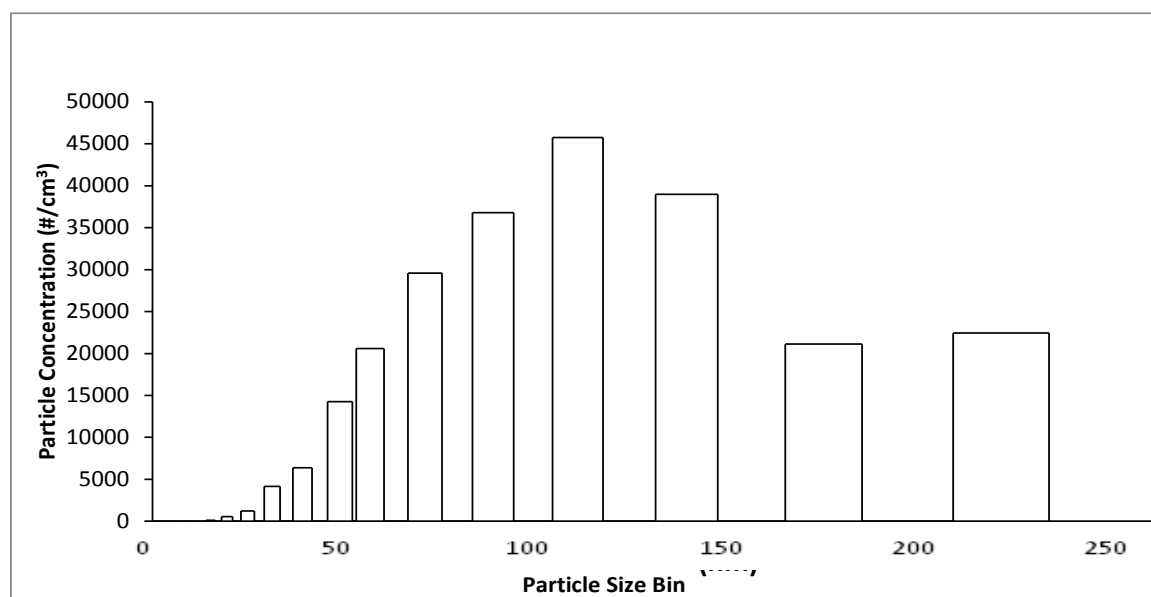


Figure 4.4: Particle number concentration data from November 23, 2015. Representing the range of particles captured in a given size bin.

[85] or calculated based on the values summarized in Table 4.2, adapted from Liu et al. [34] [11, 34, 85-87].

Approximating the air concentration this way suggests particle concentration will be high enough for the mediation of DEHP to occur, even if it does not include the entire mass concentration

4.1.4. Mass Concentration Collected on Filter. The average mass concentration, using the Fluoropore membrane filter sampling technique described in section 3.3.1.2.1,

is $2700 \pm 460 \mu\text{g}/\text{m}^3$. No filter mass was recorded during any of the deposition experiments inside the box and it does not correspond to a specific particle distribution. This technique was applied late in the project as a rough check of the mass concentration against the value calculated from number concentration distributions. After coating the box with DEHP, instrumental difficulties prevented moving forward in the project, so the deposition of the particles was reproduced in a small 5-gallon chamber. It was during a series of three small-scale experiments that the mass concentration was determined.

Table 4.2: The size distribution and concentration for typical indoor environments (T), cooking (C), and smoking (S). Mass concentration reported for room except where noted by *. Adapted from [34].

Size Bin (μm)	T (%)	C(%)			S (%)		
0-0.04	0	3	1	2	1	0	1
0.04-0.1	1	22	4	13	18	2	10
0.1-0.3	17	41	26	47	56	24	43
0.3-0.5	35	13	21	20	17	29	20
0.5-0.8	27	6	13	4	6	23	11
0.8-1	7	1	5	3	1	9	4
1-2	8	4	17	7	1	12	6
2-3	5	3	13	4	0	1	2
3-5	0	2	0	0	0	0	2
5-10	0	5	0	0	0	0	1
Mass concentration ($\mu\text{g}/\text{m}^3$)	29*	566	328	2643	116	392	63*
Reference	[85]	[88]	[85]	[86]	[87]	[78]	[13]

This technique should catch all the particles going through the system and provide a more accurate mass concentration, especially for the larger particles. Although the larger particles probably will not enhance the mass transfer of DEHP as much as the

smaller particles, the larger particles could significantly affect the deposition of particles in the chamber and contribute significantly to the total mass concentration.

4.2. PARTICLE DEPOSITION FLUX

The deposition rate of the particles is important to fully understand to ensure the particle deposition of particle-bound DEHP will not overwhelm the deposition of gas phase DEHP. Figure 4.5 depicts the mass flux of particles to the surface, with the concentration of extracted solution determined based on the conductivity of the extracted $(\text{NH}_4)_2\text{SO}_4$ solution. In this figure, the black data points represent the average of that experiment, while the white are the actual data points. Several coupons were analyzed in the same extraction solution to normalize the diversity on each coupon to achieve a higher conductivity response. Based on a linear regression, the mass flux of particles to the surface is $-0.4 \pm 0.4 \text{ mg/m}^2/\text{hr}$, but the large error makes it nearly impossible to determine any trend.

The deposition velocity was calculated from the mass accumulated as shown in equation (8) using an average mass concentration collected on the filters. Although this mass concentration may not be the correct value, it is probably of the correct order of magnitude. Figure 4.6 depicts the calculated deposition velocity graphed against the length of the experiment. The white points are the actual data points while the black points are the average of that experiment. Ideally, the deposition velocity should be constant regardless of the length of the experiment, over the examined time frames. The data suggests that some initial higher deposition is occurring, which could be the result of charged coupons inducing high deposition early on by electrophoresis of charged particles.

The particles have both positive and negative charges for an overall neutral charge. If the surfaces have any charge build-up or the particles had a charge, the particle deposition velocity would be greatly affected by this charge. Donovan et al. [89] investigated the deposition velocity of aerosol particles under various conditions. One such condition was applying various amount of electric field. In the presence of the field,

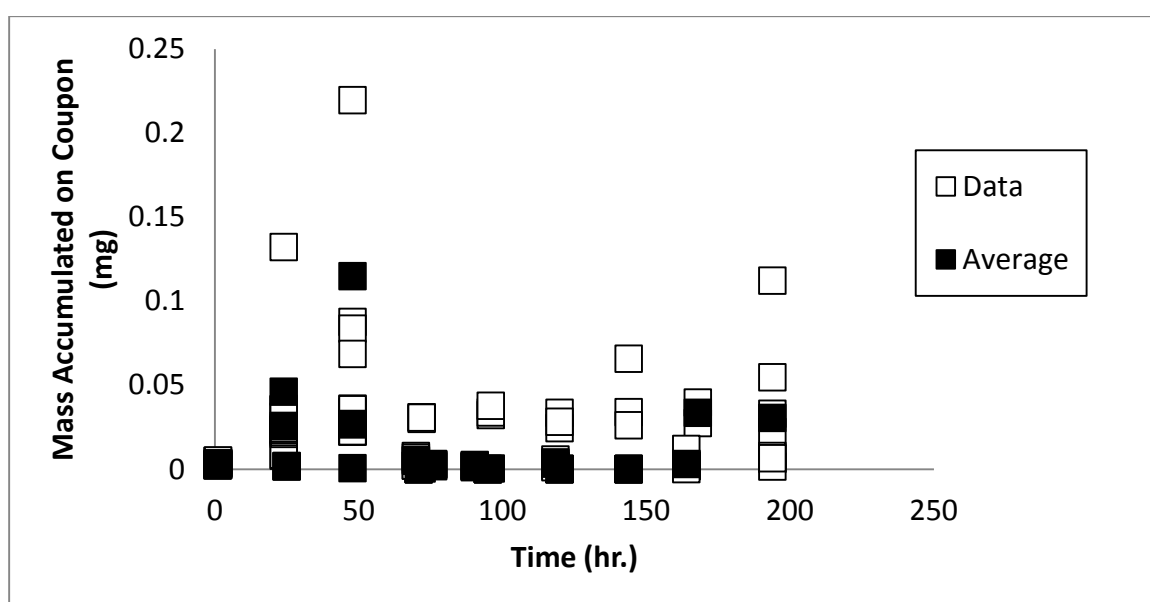


Figure 4.5: Mass accumulation of $(\text{NH}_4)_2\text{SO}_4$ per surface area over time.

they observed a strong increase in the deposition velocity. For particles with a mean diameter of 100 nm, the electric field of 100 V/cm increased the deposition velocity from 0.03 m/hr to 1.3 m/hr [89]. Nielsen and Schneider [90] also saw this effect in their investigation of electrostatic fields due to charges of surfaces, but also investigated turbulence. They found the presence of turbulence and an electrostatic field yielded a

deposition velocity ranging from 0.3 m/h to 0.03 m/h for 100 nm particles[90]. If the surface had an attractive charge build-up, the deposition velocity could be expected to increase another order of magnitude, aligning with the results of experiments with shorter than 48-hour duration. As particles of various charges deposit on the surface, this effect would be expected to diminish and normalize into a more constant deposition velocity. The box and flange were grounded to try to decrease this effect, but it did not drastically decrease the initial rapid deposition.

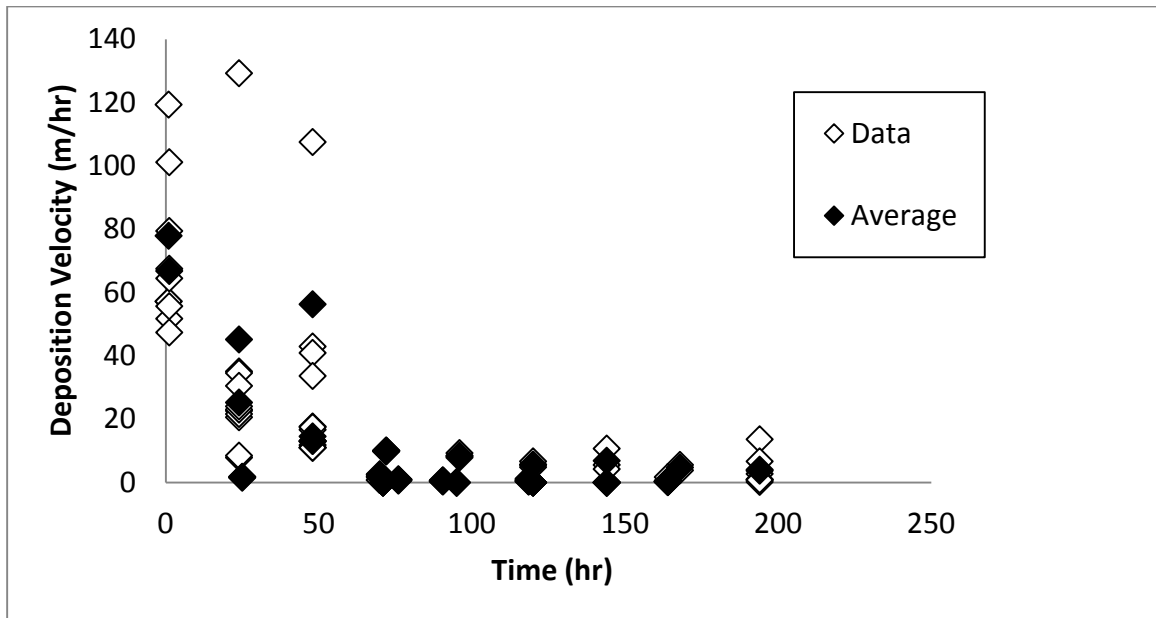


Figure 4.6: $(\text{NH}_4)_2\text{SO}_4$ deposition velocity.

The deposition velocity for the values after 70 hours align better with the average deposition velocity for particles with a mean diameter of 100 nm, Figure 4.7 represents the data for this time duration. The average deposition velocity from these experiments is

0.76 ± 0.68 m/hr. The deposition velocity is highly dependent on the particle diameter. Typically, for particles with a mean diameter of ~ 100 nm, the deposition velocity is on the order of 0.03 m/hr, which aligns with the results from this experiment [13, 66, 89, 91]. The deposition velocity seems more constant after 70 hours; future experiments should last longer than 70 hours to ensure the initial deposition of DEHP due to the particles does not overwhelm the DEHP deposition due to the enhanced mass transfer coefficient. Further, the possibility of coupon and particle charge must be addressed in future work.

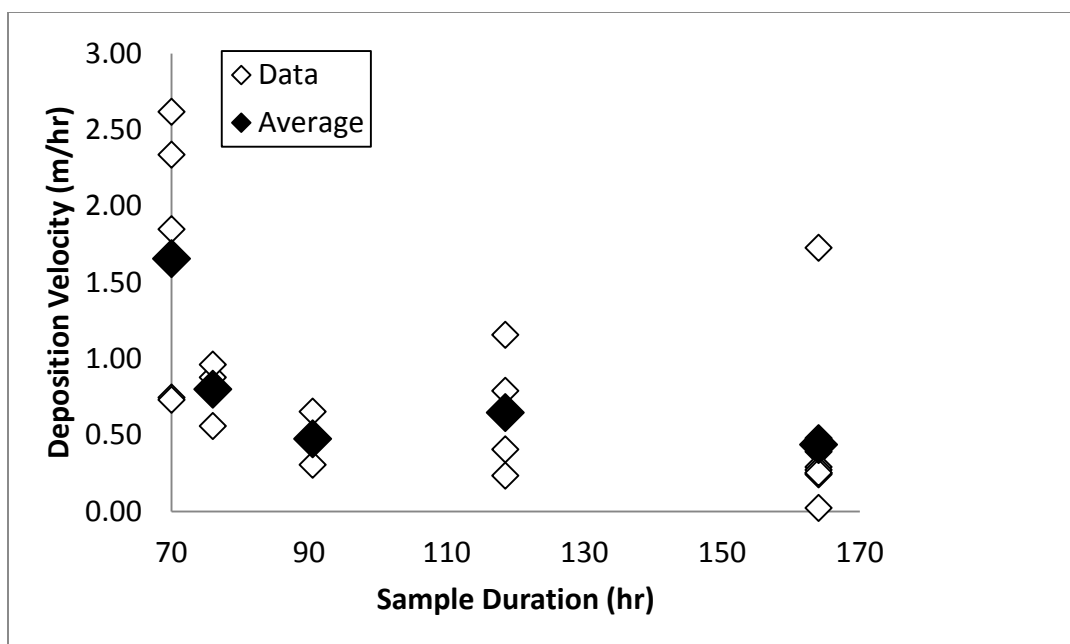


Figure 4.7: Particle deposition velocity for experiments with aduration between 70 and 170 hours.

Overall, the particle deposition velocity aligns reasonably well with typical indoor values, and the values used in the model by Liu et al. [34]. The mass concentration of the outlet stream was used in this analysis. Since the zDMA/CPC system could not quantify particles above 230 nm, it is likely that the mass concentration in the outlet stream is higher than what was recorded. Therefore, although the deposition velocity after 70 hours is still high, the method of analysis is probably accurate. In all future measurements, a mass concentration using the filter should be done for the outlet stream for each experiment and last longer than 70 hours.

4.3. ESTIMATING DEHP DEPOSITION DUE TO PARTICLE DEPOSITION

Using the dimensionless partition coefficient determined in Benning et al. [18] for DEHP to ammonium sulfate particles, the mass of DEHP deposited due to particle deposition can be determined. The dimensionless partition coefficient 5.3×10^{10} multiplied by the air concentration of DEHP and volume of particles deposited in a period of time yields the expected mass DEHP deposited due to particle deposition. Roughly 0.1 mg of particles, or $6 \times 10^{-11} \text{ m}^3$, deposited during these experiments in 400 hours. This would correspond to 3.2 μg of DEHP that would deposit with the particles. This quantity is much larger than the mass of DEHP (400 ng) that deposited in 400 hours; therefore, objective 3 was not met. Again, most of the particle deposition occurs soon after inserting coupons into the chamber, suggesting rapid accumulation of charged particles on the coupon surface. If this charging problem can be overcome, it may be possible to reduce particle-associated DEHP accumulation on coupons.

4.4. DEHP DEPOSITION VELOCITY

The deposition velocity of gas-phase DEHP in this system is important to compare to the deposition velocity without particles. Similar to the method used to estimate the deposition velocity for the particles, the mass of DEHP accumulated on a known surface area over a given time span was used to estimate the DEHP deposition velocity. Consistent characterization of this mass transfer coefficient is important to test the Liu et al. [34] model. If this value cannot be characterized in a consistent manner, the enhanced mass transfer coefficient from particles maybe within the error of the measurement values.

Unfortunately, measurements in the box were unable to be completed due to instrumentation limitations. Verification of the sampling method was instead carried out in a small 1.44-L cylindrical chamber with the inner walls thinly coated with DEHP. The coupons were magnetically held onto the lid of this can and DEHP was allowed to deposit onto the coupons.

The results for the mass depositing on the coupons per surface area, shown in Figure 4.8, suggest that mass is accumulating over time per surface area. The white triangles represent the data while the black triangles represent the average of each of the test runs. Based on two 400 h experiments, an increase in mass of DEHP on the coupons is observed. The average mass accumulated at 70 hours was 24 ± 3 ng DEHP. The average mass accumulated at 406 hours was 390 ± 76 ng DEHP. A linear regression was performed to determine the mass flux of DEHP to the surface and the 95% confidence interval. The resulting mass flux was $3.1 \times 10^3 \pm 470$ ng/m²/hr. The 95% confidence interval is approximately 15% of the measured mass flux, which meets the requirements of objective 4.

The mass accumulated on the coupons was used to estimate a deposition velocity. The air concentration of DEHP in this calculation was based on estimates of the vapor pressure for DEHP. This vapor pressure can vary, yielding air concentrations ranging from $1 \mu\text{g}/\text{m}^3$ to $2 \mu\text{g}/\text{m}^3$ [8, 92]. This small range of air concentration can impact the estimated deposition velocity for DEHP. For example, at an air concentration of $1 \mu\text{g}/\text{m}^3$, the estimated deposition velocity is $2.3 \pm 1 \text{ m/hr}$. If the air concentration is closer to $2 \mu\text{g}/\text{m}^3$, the deposition velocity estimate decreases to $1.1 \pm 0.5 \text{ m/hr}$. These values align with typical deposition velocities reported in the literature for indoor pollutants [77, 80, 93].

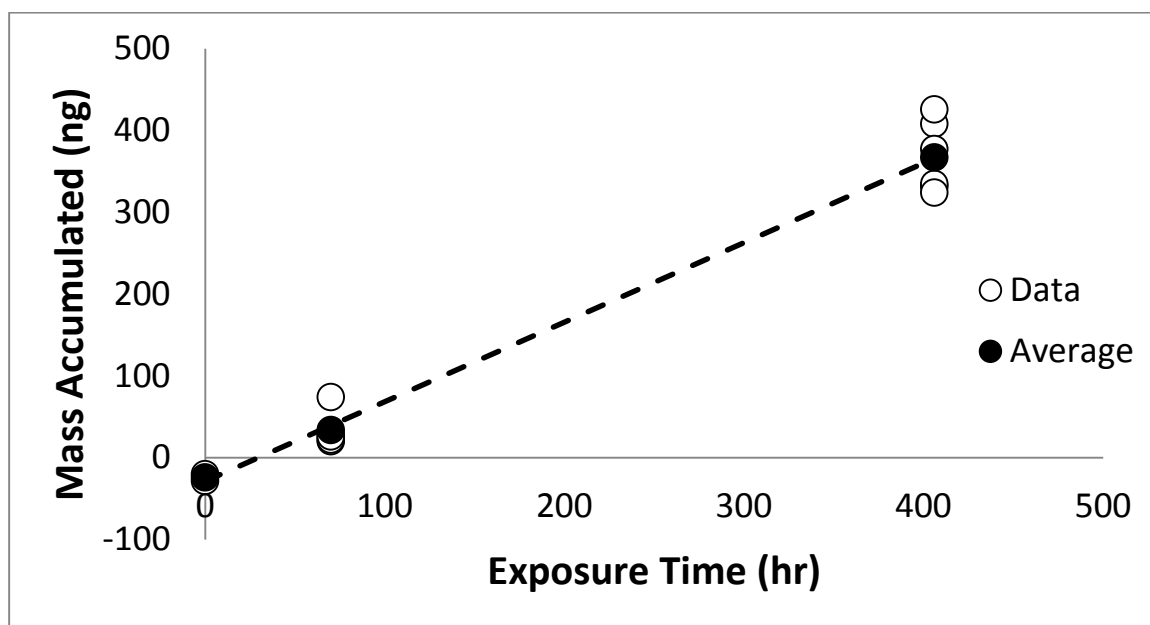


Figure 4.8: Mass of DEHP accumulated on metal coupon over time.

In a critique of the deposition velocities done by Nazaroff et al. [77], a deposition velocity for ozone reported for stainless steel room was 1.4 m/hr. Morrison et al. [79] reported a deposition velocity for ozone of 0.58-2.3 m/h onto a carpet sample. Xu and Little [80] reported two different mass transfer coefficients for DEHP in two different environments, 1.44 m/h and 5.04 m/h. These two values were measured under very different conditions than those of this sampling [80]. The comparison of these varying deposition velocities is used to emphasize that the deposition velocity is dependent on the environment of the measurement. For this reason, it will be important to characterize the deposition velocity of DEHP under the testing conditions for this experiment.

5. CONCLUSIONS

The results from these experiments did not meet all of the objectives. Estimates of the expected DEHP deposition due to particles are well above the estimates of DEHP deposition due to gas-phase deposition, failing to meet objective 3. Characterization of the particle distribution of different size bins, particle deposition, and DEHP deposition are the main check points to ensure the system can operate within the parameters suggested by model analysis performed by Liu et al. [34].

5.1. OBJECTIVE 1

The first objective was to build a system that would meet the requirements of the Liu et al. [34] model.

5.1.1. Objective 1 Conclusions. This study successfully constructed and tested a pilot scale system (sub-room scale) with ancillary flow controls, particle generation and particle measurement capabilities.

5.1.2. Objective 1 Suggestions for the Future. Since the system failed to meet objective 3, some updates to the system are warranted. The particle deposition velocity was too high, possibly due to electrophoresis. Removing the bipolar charger from the system might be useful, since this step may result in excess charge even though its intent is to develop an overall neutral charge. The particle concentration could be much higher than needed in the system. Lowering the mass concentration of particles will reduce the mass flux of particles to the surface.

5.2. OBJECTIVE 2

The second objective was to construct a particle generator that can deliver a sufficiently high concentration (50-100 $\mu\text{g}/\text{m}^3$) of polydisperse particles in the appropriate size range (10-500 nm in aerodynamic diameter) to test the Liu et al. [34] model.

5.2.1. Objective 2 Conclusions. Liu et al. [34] evaluated their model using polydisperse particle distributions, as seen in Table 4.2. The particle size distribution as measured by the zDMA/CPC resulted in a calculated concentration that is within the range used in the model by Liu et al. [34] to generate a 50% increase in mass-transfer for a compound with a dimensionless partition coefficient of 5×10^{10} . Based on the estimated size bins, number concentration, and assumed particle characteristics the inlet of the box has a mass concentration of 777 $\mu\text{g}/\text{m}^3$ with a mean particle diameter ~ 85 nm. Using this same procedure, the outlet of the box has a mass concentration of 133 $\mu\text{g}/\text{m}^3$ with a mean particle diameter ~ 105 nm. However, using a filter to collect the mass in a given air volume sample, the mass concentration at the inlet is 2700 ± 460 $\mu\text{g}/\text{m}^3$. The large difference between these two estimated mass concentrations could be due to the following:

- The system cannot quantify the concentration for particles with aerodynamic diameters greater than ~ 230 nm. Particle mass increases with the cube of the diameter and particles not observed by the device could contribute substantially to the total mass.
- The equations provided by the Cloud and Aerosol Sciences personnel may not adequately predict the “bin width” for the particle distribution

and therefore may under-count the total distribution. No other system was available to provide an independent calibration of the system during this project.

Based on the combination of measurements, the system provides a sufficiently large concentration within the size range of interest to test the Liu et al. [34] model. zDMA/CPC measurements indicate that the mass concentration is near the low-end of the required value (50-100 $\mu\text{g}/\text{m}^3$) for the size range of interest (10-500 nm in aerodynamic diameter), but filter measurements indicate that it is much greater than required.

5.2.2. Objective 2 Suggestions for the Future. The concentration of particles in the system is very important to fully characterize and understand. For this reason, a calibration check for the zDMA/CPC is necessary to ensure that the methods used to convert zDMA measurements into a complete/continuous size distribution are correct.

5.3. OBJECTIVE 3

Quantify the deposition flux and deposition velocity of the aerosol particles to metal coupons. Demonstrate that the DEHP deposition associated with particle deposition (particle bound DEHP) contributes to less than 10% of DEHP flux relative to that due to gas-phase deposition.

5.3.1. Objective 3 Conclusions. The particle deposition rate observed was higher than anticipated and may be too high to discern the gas-phase component of DEHP flux to the coupons. Mass of particles deposited was highly variable and a large fraction deposited within 1 hour of initiating an exposure. This could be due to electrostatically enhanced deposition of charged particles.

The particle deposition velocity is calculated based on the mass collected on the filter since this value should collect all particles regardless of the particle diameter. The estimated particle deposition velocity was 0.76 ± 0.68 m/h, based on the mass concentration at the outlet determined by the zDMA/CPC system. The large standard deviation in this value is probably due to variations in the actual particle mass concentration. The zDMA/CPC system cannot quantify particles above 230 nm, under-representing the true mass concentration. In all future measurements, a mass concentration done with the filter should be done for the outlet stream for each experiment. The mass concentration using the filter results in a concentration much higher than what results from the zDMA and CPC that probably better reflects the actual results.

The mass of particle bound DEHP that would deposit is well above the mass deposited by gas-phase deposition. Using the partition coefficient found by Benning et al. [18] and estimating the DEHP gas phase concentration, the mass of DEHP that would deposit due to the 0.1 mg of ammonium sulfate would be 3 μ g. This value is much higher than observed in the small chamber experiments, 390 ng of DEHP in 400 hours. Therefore, objective 3 was not met.

5.3.2. Objective 3 Suggestions for the Future. If the particle concentration is in the 2000 μ g/m³ range, the particle concentration should be decreased to prevent some of the particle deposition. In order to observe a 50% increase mass flux of DEHP, the experiment only requires 50-200 μ g/m³; therefore, this particle concentration is much higher than needed to examine this phenomenon. Since the particles seem to mostly deposit in the initial period, it could be possible to determine a baseline for the particle

bound DEHP deposition that could be subtracted from the total DEHP deposition. However, it will still be important to reduce electrostatic attraction of particles to coupons.

5.4. OBJECTIVE 4

Quantify the flux and estimate the deposition velocity of DEHP to metal coupons. Demonstrate that the flux is sufficiently reproducible to test the Liu et al. [34] model, that the 95% confidence interval is less than 30% of magnitude of the flux.

5.4.1. Objective 4 Conclusions. The flux of DEHP to coupons was measured to be $3.1 \times 10^3 \pm 470$ ng/m²/hr. Assuming the air was saturated with DEHP at 25°C, the estimated deposition velocity for gas phase DEHP ranged between 2.3 ± 1 m/h and 1.1 ± 0.5 m/h depending on the estimated air concentration, 1 µg/m³ and 2 µg/m³, respectively. The 95% confidence interval was 15% of the magnitude of the flux, which meets the requirements of objective 4.

5.4.2. Objective 4 Suggestions for the Future. Although the air concentration of DEHP is uncertain, the values determined based on the saturation concentration are within the range reported in literature. Further testing of this deposition velocity is warranted, especially for in the actual box.

The particle deposition velocity and mass concentration are well within the mass balance model developed by Liu et al. [34], suggesting that the particle mediation effect can be examined with this system. However, key challenges remain including a more accurate control and measurement of the particle concentration and distribution as well as reducing the particle mass deposited on coupons. Once these challenges are met, the system should be able to examine DEHP mass transfer due to particle mediation.

REFERENCES

1. Bekö, G., et al., *Children's Phthalate Intakes and Resultant Cumulative Exposures Estimated from Urine Compared with Estimates from Dust Ingestion, Inhalation and Dermal Absorption in Their Homes and Daycare Centers*. PLoS ONE, 2013. **8**(4): p. e62442.
2. Benning, J., et al. *Characterizing gas-particle interactions of phthalate plasticizer emitted from vinyl flooring*. in *12th International Conference on Indoor Air Quality and Climate 2011*. 2011.
3. Langer, S., et al., *Phthalate and PAH concentrations in dust collected from Danish homes and daycare centers*. Energy Conversion and Management, 2011. **52**(1): p. 108-116.
4. Little, J.C., et al., *Rapid methods to estimate potential exposure to semivolatile organic compounds in the indoor environment*. Environmental Science and Technology, 2012. **46**(20): p. 11171-11178.
5. Liu, C., et al., *The effect of ventilation on indoor exposure to semivolatile organic compounds*. Indoor Air, 2015. **25**(3): p. 285-296.
6. Morrison, G.C., et al., *Role of clothing in both accelerating and impeding dermal absorption of airborne SVOCs*. Journal of Exposure Science and Environmental Epidemiology, 2015.
7. Weschler, C.J. and W.W. Nazaroff, *SVOC exposure indoors: Fresh look at dermal pathways*. Indoor Air, 2012. **22**(5): p. 356-377.
8. Weschler, C.J. and W.W. Nazaroff, *Semivolatile organic compounds in indoor environments*. Atmospheric Environment, 2008. **42**(40): p. 9018-9040.
9. Weschler, C.J., T. Salthammer, and H. Fromme, *Partitioning of phthalates among the gas phase, airborne particles and settled dust in indoor environments*. Atmospheric Environment, 2008. **42**(7): p. 1449-1460.
10. Xu, Y., E.A. Cohen Hubal, and J.C. Little, *Predicting residential exposure to phthalate plasticizer emitted from vinyl flooring: Sensitivity, uncertainty, and implications for biomonitoring*. Environmental Health Perspectives, 2010. **118**(2): p. 253-258.
11. Xu, Y., et al., *Measuring and predicting the emission rate of phthalate plasticizer from vinyl flooring in a specially-designed chamber*. Environmental Science and Technology, 2012. **46**(22): p. 12534-12541.

12. Xu, Y., et al. *Characterizing emissions of phthalate plasticizer from vinyl flooring in a specially-designed SVOC emission chamber*. in *9th International Conference and Exhibition - Healthy Buildings 2009, HB 2009*. 2009.
13. Nazaroff, W.W., *Indoor particle dynamics*. Indoor Air, Supplement, 2004. **14**(SUPPL. 7): p. 175-183.
14. Latini, G., A. Verrotti, and C. De Felice, *DI-2-ethylhexyl phthalate and endocrine disruption: A review*. Current Drug Targets: Immune, Endocrine and Metabolic Disorders, 2004. **4**(1): p. 37-40.
15. Kay, V.R., M.S. Bloom, and W.G. Foster, *Reproductive and developmental effects of phthalate diesters in males*. Critical Reviews in Toxicology, 2014. **44**(6): p. 467-498.
16. Heger, N.E., et al., *Human fetal testis xenografts are resistant to phthalate-induced endocrine disruption*. Environmental Health Perspectives, 2012. **120**(8): p. 1137-1143.
17. Romani, F., et al., *Endocrine disruptors and human reproductive failure: The in vitro effect of phthalates on human luteal cells*. Fertility and Sterility, 2014. **102**(3): p. 831-837.
18. Benning, J.L., et al., *Characterizing gas-particle interactions of phthalate plasticizer emitted from vinyl flooring*. Environmental Science and Technology, 2013. **47**(6): p. 2696-2703.
19. Liu, Z. and J.C. Little, *Semivolatile organic compounds (SVOCs): Phthalates and flame retardants*, in *Toxicity of Building Materials*. 2012. p. 122-137.
20. Liu, Z., Y. Xu, and J.C. Little. *Characterizing emissions of di-2-ethylhexyl phthalate from vinyl flooring in a specially-designed chamber*. in *12th International Conference on Indoor Air Quality and Climate 2011*. 2011.
21. Liu, Z., W. Ye, and J.C. Little, *Predicting emissions of volatile and semivolatile organic compounds from building materials: A review*. Building and Environment, 2013. **64**: p. 7-25.
22. Cheng, K.C., M.D. Goebes, and L.M. Hildemann, *Association of size-resolved airborne particles with foot traffic inside a carpeted hallway*. Atmospheric Environment, 2010. **44**(16): p. 2062-2066.
23. Hussein, T., et al., *Particle size characterization and emission rates during indoor activities in a house*. Atmospheric Environment, 2006. **40**(23): p. 4285-4307.
24. Nasir, Z.A. and I. Colbeck, *Particulate pollution in different housing types in a UK suburban location*. Science of the Total Environment, 2013. **445-446**: p. 165-176.

25. Thatcher, T.L. and W.W. Nazaroff, *Effect of small-scale obstructions and surface textures on particle deposition from natural convection flow*. Aerosol Science and Technology, 1997. **27**(6): p. 709-725.
26. Martuzevicius, D., et al., *Resuspension of particulate matter and PAHs from street dust*. Atmospheric Environment, 2011. **45**(2): p. 310-317.
27. McMeeking, G.R., *Size Distribution Measurements of Wildfire Smoke-Influenced Aerosol at Yosemite National Park*, in *Department of Atmospheric Science*. 2004, Colorado State University: Fort Collins, Colorado. p. 121.
28. Shaughnessy, R. and H. Vu, *Particle loadings and resuspension related to floor coverings in chamber and in occupied school environments*. Atmospheric Environment, 2012. **55**: p. 515-524.
29. Wang, S., et al., *An experimental study on short-time particle resuspension from inner surfaces of straight ventilation ducts*. Building and Environment, 2012. **53**: p. 119-127.
30. Sippola, M.R., R.G. Sextro, and T.L. Thatcher, *Measurements and modeling of deposited particle transport by foot traffic indoors*. Environmental Science and Technology, 2014. **48**(7): p. 3800-3807.
31. Cousins, I.T., A.J. Beck, and K.C. Jones, *A review of the processes involved in the exchange of semi-volatile organic compounds (SVOC) across the air-soil interface*. Science of the Total Environment, 1999. **228**(1): p. 5-24.
32. Xu, Y., et al., *Predicting residential exposure to phthalate plasticizer emitted from vinyl flooring: A mechanistic analysis*. Environmental Science and Technology, 2009. **43**(7): p. 2374-2380.
33. Asgharian, B., O.T. Price, and W. Hofmann, *Prediction of particle deposition in the human lung using realistic models of lung ventilation*. Journal of Aerosol Science, 2006. **37**(10): p. 1209-1221.
34. Liu, C., G.C. Morrison, and Y. Zhang, *Role of aerosols in enhancing SVOC flux between air and indoor surfaces and its influence on exposure*. Atmospheric Environment, 2012. **55**: p. 347-356.
35. Liu, C., B. Zhao, and Y. Zhang, *The influence of aerosol dynamics on indoor exposure to airborne DEHP*. Atmospheric Environment, 2010. **44**(16): p. 1952-1959.
36. Chen, Q. and K. Hu, *Prediction model for SVOCs transport in the air and interactions with airborne particles*. Atmospheric Environment, 2014. **96**: p. 61-69.

37. Lewis, W.K. and W.G. Whitman, *Principles of Gas Absorption*. Industrial and Engineering Chemistry, 1924. **16**(12): p. 1215-1220.
38. Ueda, H. and G. Havenith, *The effect of fabric air permeability on clothing ventilation*, in *Elsevier Ergonomics Book Series*. 2005. p. 343-346.
39. Chemspider, *Chemspider CSID: 10379*. 2014: <http://www.chemspider.com/Chemical-Structure.10379.html>CSID:10379 (accessed 20:07, May 25, 2014).
40. Morrison, G., et al., *Role of Clothing in both increasing and decreasing dermal absorption of airborne SVOCs*. TBA, TBA.
41. Morrison, G., N.V. Shakila, and K. Parker, *Accumulation of gas-phase methamphetamine on clothing, toy fabrics, and skin oil*. Indoor Air, 2014.
42. Zhang, Y., et al., *The influence of facility agriculture production on phthalate esters distribution in black soils of northeast China*. Science of the Total Environment, 2015. **506-507**: p. 118-125.
43. Pan, T.L., et al., *Dermal toxicity elicited by phthalates: Evaluation of skin absorption, immunohistology, and functional proteomics*. Food and Chemical Toxicology, 2014. **65**: p. 105-114.
44. Posnack, N.G., *The Adverse Cardiac Effects of Di(2-ethylhexyl)phthalate and Bisphenol A*. Cardiovascular Toxicology, 2014.
45. Ghosh, J., et al., *Hepatotoxicity of di-(2-ethylhexyl)phthalate is attributed to calcium aggravation, ROS-mediated mitochondrial depolarization, and ERK/NF- κ B pathway activation*. Free Radical Biology and Medicine, 2010. **49**(11): p. 1779-1791.
46. Tran, B.C., et al., *BPA and phthalate fate in a sewage network and an elementary river of France. Influence of hydroclimatic conditions*. Chemosphere, 2015. **119**: p. 43-51.
47. Cai, Q.Y., et al., *Genotypic variation in the uptake, accumulation, and translocation of di-(2-ethylhexyl) phthalate by twenty cultivars of rice (*Oryza sativa* L.)*. Ecotoxicology and Environmental Safety, 2015. **116**: p. 50-58.
48. Yang, Y., et al., *Determination of phthalate plasticizers in daily foods and their migration from food packages*. Se pu = Chinese journal of chromatography / Zhongguo hua xue hui, 2013. **31**(7): p. 674-678.
49. Morrison, G., et al., *Airborne phthalate partitioning to cotton clothing*. Atmospheric Environment, 2015. **115**(0): p. 149-152.

50. Koniecki, D., et al., *Phthalates in cosmetic and personal care products: Concentrations and possible dermal exposure*. Environmental Research, 2011. **111**(3): p. 329-336.
51. Shin, I.-S., et al., *Effects of maternal exposure to di(2-ethylhexyl)phthalate (DEHP) during pregnancy on susceptibility to neonatal asthma*. Toxicology and Applied Pharmacology, 2014. **274**(3): p. 402-407.
52. Shi, S. and B. Zhao, *Modeled exposure assessment via inhalation and dermal pathways to airborne semivolatile organic compounds (SVOCs) in residences*. Environmental Science and Technology, 2014. **48**(10): p. 5691-5699.
53. Net, S., et al., *Reliable quantification of phthalates in environmental matrices (air, water, sludge, sediment and soil): A review*. Science of the Total Environment, 2015. **515-516**: p. 162-180.
54. Xie, Z., et al., *Atmospheric concentrations and air-sea exchanges of phthalates in the North Sea (German Bight)*. Atmospheric Environment, 2005. **39**(18): p. 3209-3219.
55. Koch, H.M. and A.M. Calafat, *Human body burdens of chemicals used in plastic manufacture*. Philosophical Transactions of the Royal Society B: Biological Sciences, 2009. **364**(1526): p. 2063-2078.
56. Rubin, R.J. and R.J. Jaeger, *Some pharmacologic and toxicologic effects of di-2-ethylhexyl phthalate (DEHP) and other plasticizers*. Environmental Health Perspectives, 1973. **3**: p. 53-59.
57. Teil, M.J., M. Blanchard, and M. Chevreuil, *Atmospheric fate of phthalate esters in an urban area (Paris-France)*. Science of the Total Environment, 2006. **354**(2-3): p. 212-223.
58. Werner, E.F., et al., *The association between maternal urinary phthalate concentrations and blood pressure in pregnancy: The HOME Study*. Environmental Health: A Global Access Science Source, 2015. **14**(1).
59. Mu, D., et al., *Levels of Phthalate Metabolites in Urine of Pregnant Women and Risk of Clinical Pregnancy Loss*. Environmental Science and Technology, 2015. **49**(17): p. 10651-10657.
60. Ferguson, K.K., et al., *Variability in urinary phthalate metabolite levels across pregnancy and sensitive windows of exposure for the risk of preterm birth*. Environment International, 2014. **70**: p. 118-124.
61. Salthammer, T., et al., *Effect of particle concentration and semi-volatile organic compounds on the phenomenon of 'black magic dust' in dwellings*. Building and Environment, 2011. **46**(10): p. 1880-1890.

62. Schripp, T., I. Kirsch, and T. Salthammer, *Characterization of particle emission from household electrical appliances*. Science of the Total Environment, 2011. **409**(13): p. 2534-2540.
63. Zuo, B., K. Zhong, and Y. Kang, *An experimental study on particle resuspension in a room with impinging jet ventilation*. Building and Environment, 2015. **89**: p. 48-58.
64. Thatcher, T.L. and D.W. Layton, *Deposition, resuspension, and penetration of particles within a residence*. Atmospheric Environment, 1995. **29**(13): p. 1487-1497.
65. Holländer, W. and W. Stöber, *Aerosols of smoke, respiratory physiology and deposition*. Archives of toxicology. Supplement. Archiv fur Toxikologie. Supplement, 1986. **9**: p. 74-87.
66. You, R., B. Zhao, and C. Chen, *Developing an empirical equation for modeling particle deposition velocity onto inclined surfaces in indoor environments*. Aerosol Science and Technology, 2012. **46**(10): p. 1090-1099.
67. Thatcher, T.L., et al., *Effects of room furnishings and air speed on particle deposition rates indoors*. Atmospheric Environment, 2002. **36**(11): p. 1811-1819.
68. Edwards, R.D., E.J. Yurkow, and P.J. Lioy, *Seasonal deposition of housedusts onto household surfaces*. Science of the Total Environment, 1998. **224**(1-3): p. 69-80.
69. Cousins, I.T. and D. Mackay, *Gas - Particle partitioning of organic compounds and its interpretation using relative solubilities*. Environmental Science and Technology, 2001. **35**(4): p. 643-647.
70. Junge, C.E., *BASIC CONSIDERATIONS ABOUT TRACE CONSTITUENTS IN THE ATMOSPHERE AS RELATED TO THE FATE OF GLOBAL POLLUTANTS*. Adv Environ Sci Technol, 1975. **8**: p. 7-25.
71. Goss, K.U. and R.P. Schwarzenbach, *Gas/solid and gas/liquid partitioning of organic compounds: Critical evaluation of the interpretation of equilibrium constants*. Environmental Science and Technology, 1998. **32**(14): p. 2025-2032.
72. Pankow, J.F., *Review and comparative analysis of the theories on partitioning between the gas and aerosol particulate phases in the atmosphere*. Atmospheric Environment (1967), 1987. **21**(11): p. 2275-2283.
73. Yamasaki, R.S., *SURFACE WEATHERABILITY OF GLASS-FIBER REINFORCED POLYESTER SHEETING - 2. EFFECT OF CONSTITUENTS*. Composites technology review, 1982. **4**(4): p. 125-129.

74. Liu, C., et al., *Analysis of the dynamic interaction between SVOCs and airborne particles*. Aerosol Science and Technology, 2013. **47**(2): p. 125-136.
75. Cano-Ruiz, J.A., et al., *Removal of reactive gases at indoor surfaces: Combining mass transport and surface kinetics*. Atmospheric Environment Part A, General Topics, 1993. **27**(13): p. 2039-2050.
76. Nazaroff, W.W. and G.R. Cass, *Mass-transport aspects of pollutant removal at indoor surfaces*. Environment International, 1989. **15**(1-6): p. 567-584.
77. Nazaroff, W.W., A.J. Gadgil, and C.J. Weschler. *Critique of the use of deposition velocity in modeling indoor air quality*. in *ASTM Special Technical Publication*. 1993.
78. Nazaroff, W.W., et al., *Predicting regional lung deposition of environmental tobacco smoke particles*. Aerosol Science and technology, 1993. **19**: p. 243-254.
79. Morrison, G.C. and W.W. Nazaroff, *The rate of ozone uptake on carpet: Mathematical modeling*. Atmospheric Environment, 2002. **36**(11): p. 1749-1756.
80. Xu, Y. and J.C. Little, *Predicting emissions of SVOCs from polymeric materials and their interaction with airborne particles*. Environmental Science and Technology, 2006. **40**(2): p. 456-461.
81. Ferreira, A., et al., *Temperature and solid properties effects on gas-liquid mass transfer*. Chemical Engineering Journal, 2010. **162**(2): p. 743-752.
82. Littlejohns, J.V. and A.J. Daugulis, *Oxygen transfer in a gas-liquid system containing solids of varying oxygen affinity*. Chemical Engineering Journal, 2007. **129**(1-3): p. 67-74.
83. Kim, J., P. Moin, and R. Moser, *Turbulence statistics in fully developed channel flow at low Reynolds number*. Journal of Fluid Mechanics, 1987. **177**: p. 133-166.
84. Cussler, E.L., *Diffusion*. Second ed. 1997: Cambridge University Press.
85. See, S.W. and R. Balasubramanian, *Risk assessment of exposure to indoor aerosols associated with Chinese cooking*. Environmental Research, 2006. **102**(2): p. 197-204.
86. Wallace, L.A., S.J. Emmerich, and C. Howard-Reed, *Source Strengths of Ultrafine and Fine Particles Due to Cooking with a Gas Stove*. Environmental Science and Technology, 2004. **38**(8): p. 2304-2311.
87. Klepeis, N.E., et al., *Determining size-specific emission factors for environmental tobacco smoke particles*. Aerosol Science and Technology, 2003. **37**(10): p. 780-790.

88. Buonanno, G., L. Morawska, and L. Stabile, *Particle emission factors during cooking activities*. Atmospheric Environment, 2009. **43**(20): p. 3235-3242.
89. Donovan, R.P., T. Yamamoto, and R. Periasamy. *Particle deposition, adhesion, and removal*. in *Materials Research Society Symposium Proceedings*. 1993.
90. Nielsen, N.F. and T. Schneider, *Particle Deposition onto a Human Head: Influence of Electrostatic and Wind Fields*. Bioelectromagnetics, 1998. **19**(4): p. 246-258.
91. Yook, S.J., C. Asbach, and K.H. Ahn, *Particle deposition velocity onto a face-up flat surface in a laminar parallel flow considering Brownian diffusion and gravitational settling*. Journal of Aerosol Science, 2010. **41**(10): p. 911-920.
92. EPA, U. *Bis(2ethylhexyl) phthalate (DEHP) / Technology Transfer Network Air Toxics Web site / US EPA*. 9/10/2015 2/10/2016]; Available from: <http://www3.epa.gov/airtoxics/hlthef/eth-phth.html>.
93. Morrison, G.C., et al., *Rapid measurement of indoor mass-transfer coefficients*. Atmospheric Environment, 2003. **37**(39-40): p. 5611-5619.

VITA

Melissa Buechlein was born in St. Louis, Missouri. In May 2014, she received her B.S. with Honors in Environmental Engineering from the Missouri University of Science and Technology, Rolla, Missouri. In May 2016, she received her M.S. in Environmental Engineering from the Missouri University of Science and Technology, Rolla, Missouri.

Melissa has published conference and coauthored journal papers. She has also presented at national and international conferences. Melissa was awarded the Chancellor's Fellowship in July 2014 to fund her M.S. in Environmental Engineering.